Abstract

Using Mößbauer spectroscopy, in this experiment two absorber materials – stainless steel and natural iron – are investigated and several properties of the nuclear energy levels are determined. In addition to the observation of isomeric shift and hyperfine structure, as well as the associated magnetic field and moment, the effective absorber thickness and the fraction of recoilless absorptions, known as the Debye-Waller factor are determined. In a last step, using the linewidth of the peaks, the lifetime of the energy level can be found. In addition, three models for the peak fitting are compared – the Gauß, Lorentz and Voigt profile.

For natural iron, the isomeric shift is determined to be $E_{\text{iso}} = (10.1 \pm 1.3)\,\text{neV}$, an effective absorber thickness of $T_A = 6.4 \pm 0.5$ and a Debye-Waller factor of $f_Q = 0.381 \pm 0.015$ are found and the lifetime is computed to be $\tau = (110 \pm 20)\,\text{ns}$. All values are found using the Lorentz profile. Using the other fit functions, comparable results are found. For natural iron, the isomeric shift is given by $E_{\text{iso}} = (4.5 \pm 1.1)\,\text{neV}$ and the hyperfine structure can be resolved, finding a magnetic field of $B = (32.6 \pm 1.4)\,\text{T}$ and a nuclear magnetic moment of $\mu_e = (-0.160 \pm 0.012)$. The effective absorber thickness of $T_A = 9.0 \pm 0.3$ is here weighted for every peak, resulting in Debye-Waller factors ranging from 5 % to 20 %. For the lifetime, a great variety of values was found, depending on peak and fitting model, with all values having a significant relative error.

Contents

List of Tables

List of Figures

1 Introduction

Emission and reabsorption of γ radiation in nuclear transitions is already known since the early 20th century. However, a measurement of the transitions was not possible for a long time. This is due to a recoil in the emission material, where energy gets lost being transferred to the momentum of the nucleus. A first solution was proposed by Rudolf Mößbauer in 1957, who discovered recoilless emission, when the involved nucleus is bound in a lattice. This phenomenon is known as the Mößbauer effect.

Nowadays, Mößbauer spectroscopy is a powerful tool to investigate nuclear energy levels of solids. Here, the linewidth of the detected spectrum originates from the state's natural lifetime and not from Doppler broadening due to the recoilless emission. This allows the determination of further nuclear properties as the lifetime. In connection with the relativistic Doppler effect, it is moreover possible to vary the energy of emitted γ radiation in the order of neV, which allows a very fine spectral resolution of an absorption spectrum. Therefore, the discovery of the Mößbauer effect lead to new possibilities in spectroscopy [1]. Nowadays, it is used in several applications, as for example investigation of materials on mars with NASA's rover spirit [2].

In this experiment, Mößbauer spectroscopy is used to study the absorption spectra of stainless steel and natural iron. As a γ source, a ^{57}Co sample was used, which decays via electron capture in ^{57}Fe, emitting γ radiation of 14.4 keV. With this radiation, the isomeric shift of the nuclear levels in stainless steel and natural iron will be examined. Moreover, we determine the effective absorber thickness, the Debye-Waller factor and the lifetime of the states of stainless steel and natural iron. In addition, we study the hyperfine splitting of the nuclear states of natural iron and with these determine the internal magnetic field $\vec{B}$ and magnetic moment μ.

2 Theory

In the following, a short overview of the theoretical background relevant for this experiment is given. This includes the relativistic Doppler effect, radioactive decays of the used sources, the connection between linewidth and lifetime, the isomeric shift, hyperfine structure, interactions of γ radiation and matter and the Mößbauer effect.

2.1 Relativistic Doppler effect

This section about the relativistic Doppler shift is based on Ref. [3]. For the emission or absorption of γ radiation, the energy of the photon in the reference frame of the emitter or absorber respectively is relevant. If the absorber moves away from the emitter, with relative velocity v, the frequency f_a in the absorber rest frame is Doppler shifted from the emitted frequency f_e in the emitter rest frame in the following way:

$$f_a = \sqrt{\frac{1-\frac{v}{c}}{1+\frac{v}{c}}} \cdot f_e, \tag{1}$$

$$\approx \left(1-\frac{v}{c}\right) \cdot f_e, \tag{2}$$

where c is the speed of light and the second line results from a Taylor expansion to first order. As the photon energy is given by $E = hf$ with h the Planck constant, it follows:

$$E_a \approx \left(1-\frac{v}{c}\right) \cdot E_e, \tag{3}$$

$$\Rightarrow \Delta E = \frac{v}{c} \cdot E_e. \tag{4}$$

The energy difference is positive, if the absorber moves away from the emitter and negative when it moves towards it. In this experiment the Doppler effect is used to achieve small energy differences ΔE from the emission energy by moving the absorber. With velocities in order of $\mathrm{mm\,s^{-1}}$ it is possible to get an energy resolution in neV.

2.2 γ radiation

2.2.1 Decays of the used source

We use a ^{57}Co source to get the γ radiation for the spectroscopy. ^{57}Co decays via electron capture into an excited state of ^{57}Fe. In electron capture processes, an electron from an inner atomic shell and a proton of the nucleus transform into a neutron and a neutrino:

$$p^+ + e^- \rightarrow n^0 + \nu_e^0. \tag{5}$$

Therefore, the number of nucleons stays constant, but the proton number reduces and the neutron number raises by one [4]. The excited ^{57}Fe state decays either directly into the ground state or first into an intermediate state and then to the ground state. The photon emitted from the intermediate state has an energy of 14.4 keV and is here used for Mößbauer spectroscopy. The decay scheme of ^{57}Co can be seen in Figure 1 and is taken from [5].

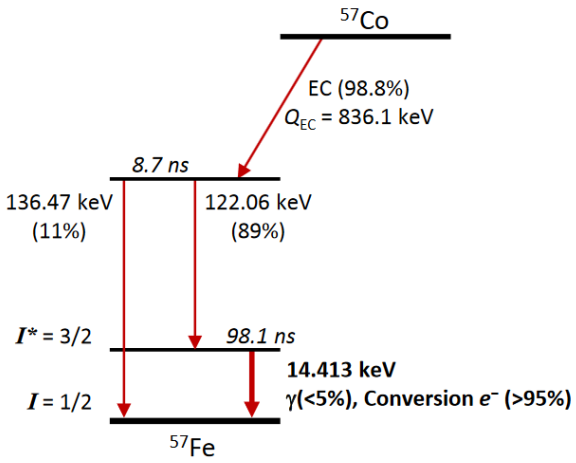

Fig. 1: The decay scheme of ^{57}Co is shown. The graphic is taken from [5]. The electron capture process from ^{57}Co to ^{57}Fe, as well as the γ decays of excited ^{57}Fe states to the ground state.

2.2.2 Linewidth and lifetimes

The lifetime τ of a nuclear state is connected to the natural linewidth Γ_0 of the emission spectrum in the following way: $\tau = \frac{\hbar}{\Gamma_0}$. This connection can be motivated by the Heisenberg uncertainty principle [6]:

$$\Delta E \Delta t \geq \hbar. \tag{6}$$

The emitted photon energy is Lorentz distributed with full width half maximum (FWHM) Γ_0. In our experimental situation, we do not only have one emission of the spectrum but also an absorption and re-emission in the used absorber. If the emitter and absorber are assumed to be thin, the radiation is only one time absorbed and re-emitted. Therefore, the measured linewidth is $\Gamma = 2\Gamma_0$. In the more general case of a finitely thick emission and absorption material, this has

to be corrected using the effective absorber thickness T_A. In Ref. [7], the correction is estimated to be:

$$\Gamma = 2\Gamma_0 \cdot \left(1 + 0.1288 T_A + 4.733 \times 10^{-3} T_A^2 - 9.21 \times 10^{-4} T_A^3 + 3.63 \times 10^{-5} T_A^4\right). \tag{7}$$

The effective absorber thickness is hereby defined as follows [8]:

$$T_A = f_A n_A \beta \sigma d, \tag{8}$$

with f_A the probability of a resonant recoilless emission (Debye-Waller factor), n_A the number density of atoms the element, β the fraction of the isotope in the element, d the thickness of the absorber and σ the cross section at resonance. Thus, the effective absorber thickness is a measure of recoilless interactions between γ radiation and the absorber. The cross section σ can be calculated with [7]:

$$\sigma = \frac{\lambda^2}{2\pi} \cdot \frac{2I^* + 1}{2I + 1} \cdot \frac{1}{1 + \alpha}, \tag{9}$$

where I^* and I are the nuclear spins of the excited and the ground state, λ the wavelength of the photon and α the conversion coefficient of the transition. If there is an additional line splitting in the absorber, as in the case of natural iron, the absorber thickness has to be corrected for every peak with the relative intensity $W_i = \frac{I_i}{\sum_j I_j}$ [8]:

$$T_{A,i} = W_i \cdot T_A. \tag{10}$$

2.2.3 Isomeric shift and hyperfine structure

In the following, we will discuss two effects which affect the nuclear energy levels. These are the isomeric shift and the hyperfine structure.

The isomeric shift results from perturbations of the Hamiltonian, rising from the fact that the nucleus is not point like but rather has a finite charge distribution [9, 10]. Moreover, the electron density in the nucleus is taken into account. Considering these distributions, for example via perturbation theory, theoretically predicts a shift of the energy levels. This shift is called isomeric shift. The isomeric shift can provide information on the chemical properties of the material.

Additionally, the energy levels in natural iron are splitted by the magnetic field $\vec{B}$ of the shell electrons. This is due to the broken symmetry in the Hamiltonian, because the magnetic field $\vec{B}$ assigns a quantization axis of the angular momentum I. The magnetic quantum number m_I corresponding to this axis characterizes the now undegenerate energy states E_i. The energy levels are shifted by:

$$E_{\text{hyperfine}} = -\frac{\mu m_I B}{I}, \tag{11}$$

with μ the magnetic moment, m_I and I the magnetic quantum numbers and B the absolute value of the internal magnetic field. The excitation energies from a state with I_1, m_1 to another state with I_2, m_2 is therefore given by:

$$\Delta E_{(I_1,m_1)\to(I_2,m_2)} = (E_{I_2} - E_{I_1}) + E_{\text{iso}} + \left(-\frac{\mu_e m_2}{I_2} + \frac{\mu_g m_1}{I_1}\right) B, \tag{12}$$

where μ_e is the magnetic moment of the excited and μ_g the magnetic moment in the ground state. The first term corresponds to the energy difference without corrections, the second term results from the isomeric shift and the last term from the hyperfine splitting.

We now consider the special case of the ^{57}Fe nuclei in natural iron. The hyperfine splitting of the energy levels here takes the form depicted in Figure 2. Moreover, the expected spectrum can be seen and the peaks are assigned to the transitions.

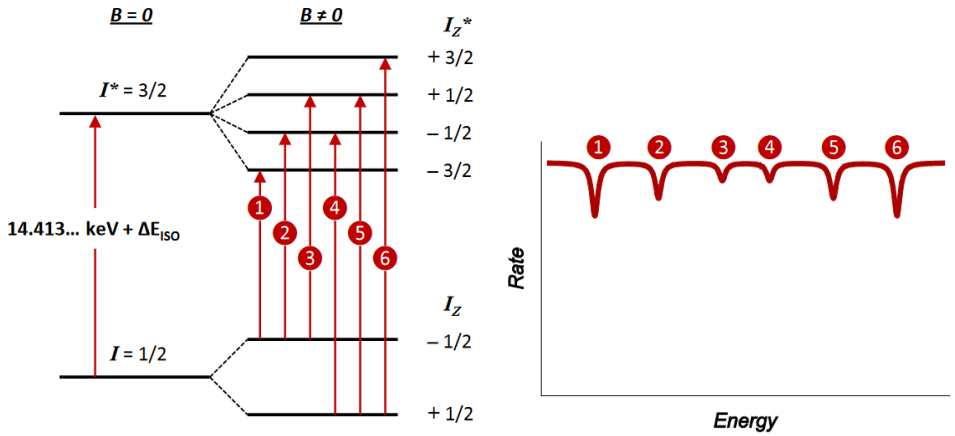

Fig. 2: The graphic shows the hyperfine splitting of the ground and first excited state of ^{57}Fe. Moreover, the expected absorption spectrum is plotted to show the assignment of the transitions and the absorption spectrum. The labeling differs from the labeling used in this protocol. The figure is taken from [11].

In the following, the peaks are labeled differently: Starting from the center, the peaks are numbered and labeled by left or right. As an example for the energy shift, in the following, we consider the inner right peak. The difference of the transition energy with and without hyperfine splitting is given by :

$$E_1 = \Delta E_{(1/2,+1/2)\to(3/2,-1/2)} - (E_{I_2} - E_{I_1} + E_{\text{iso}})\,, \tag{13}$$

$$= \left(-\frac{\mu_e m_2}{I_2} + \frac{\mu_g m_1}{I_1}\right) B, \tag{14}$$

$$= \left(-\frac{-\frac{1}{2}\mu_e}{\frac{3}{2}} + \frac{+\frac{1}{2}\mu_g}{\frac{1}{2}}\right) B, \tag{15}$$

$$= \left(\mu_g + \frac{\mu_e}{3}\right) B. \tag{16}$$

For the other peaks on the right side, it follows analogously:

$$E_2 = (\mu_g - \frac{1}{3}\mu_e) \cdot B, \tag{17}$$

$$E_3 = (\mu_g - \mu_e) \cdot B. \tag{18}$$

The energy differences for the peaks on the left side only differ in their sign.

2.2.4 Interaction with matter

To understand interactions of γ radiation with matter, which occur in the detection and the experimental setup, we shortly discuss four main effects. The paragraph is based on Ref. [12].

Photoelectric effect

For low photon energies E_γ, the photoelectric effect dominates the absorption. The photon is absorbed by an electron in the atomic shell of the material. The electron is thereby extracted

from the atom and the free electron has the kinetic energy of $E_e = E_\gamma - E_B$, with E_B the binding energy. This effect gets inefficient for high photon energies. Therefore, it does not contribute significantly to the absorption in this experiment.

Compton scattering

In this experiment, the main effect of matter-radiation interaction is the Compton scattering. Here, the photon scatters inelastically with electrons. This means that the photon loses energy through the scattering. In the experiment, this leads to a Compton background, because there are also higher energetic γ decays of ^{57}Fe which may have the same energy as the 14.4 keV photons after they have undergone Compton scattering. Those scattered electrons would be mistakenly detected.

e^--e^+ pair production

For photon energies greater than two electron masses $E_\gamma > 1022\,\text{keV}$ [13], it is possible, that the photon creates an e^--e^+ pair. Due to momentum conservation this is only possible in the field of an atom. The pair production energy is clearly higher than the energies relevant in this experiment and the pair production has no influence on the γ radiation here.

As seen in the previous discussion, the dominating interaction process of γ radiation with matter depends on the photon energy E_γ. The absorption cross section can be seen in Figure 3. It is a measure for the probability of the interaction.

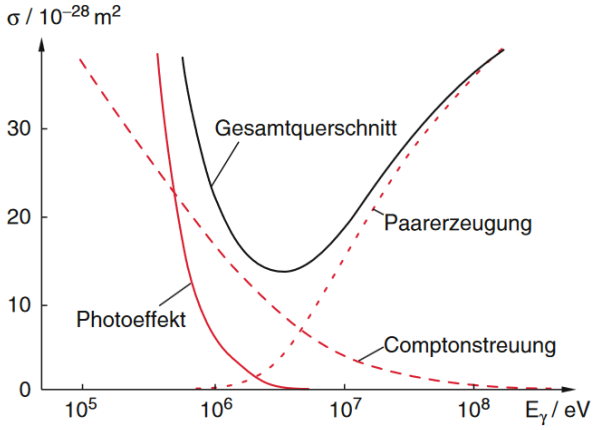

Fig. 3: The graphic shows the absorption cross section in dependence of the photon energy E_γ. The contributions of Photo effect (Photoeffekt), Compton effect (Comptoneffekt) and Pair production (Paarerzeugung) are shown, as well as the total cross section (Gesamtquerschnitt). The picture is taken from Ref. [12].

Attenuation of γ radiation

Another effect, which has to be taken into account, is the attenuation of γ radiation in acrylic glass, as the absorbers in this experiments are covered by two plates of this material. The intensity of the radiation decreases exponentially through the acrylic glass. The relative intensity after an absorber of thickness d, density ρ and absorption coefficient μ/ρ is called transition T and can be calculated by:

$$T := \frac{I}{I_0} = \exp\left(-\frac{\mu}{\rho}\rho d\right), \tag{19}$$

with I_0 the incoming and I the outgoing intensity [14].

2.3 The Mößbauer effect

At last, we discuss the Mößbauer effect in more detail as described in Ref. [15]. When a nucleus decays via a γ decay, energy and momentum has to be conserved. We first discuss this in the non-relativistic limit for a two particle decay. Here, the conservation laws demand the following equalities:

$$E_2 = E_1 + \frac{mv^2}{2} + hf, \tag{20}$$

$$0 = mv + \frac{hf}{c}, \tag{21}$$

where E_2 is the energy of the excited nuclear state, E_1 the energy of the de-excited state, m the mass of the nucleus, v the velocity of the nucleus after the decay, h Planck's constant and c the speed of light. So the energy of the emitted photon is:

$$hf = (E_2 - E_1) - \frac{h^2 f^2}{2mc^2}, \tag{22}$$

$$=: (E_2 - E_1) - R. \tag{23}$$

Here, it is clearly visible that the energy of the photon is always smaller than the energy difference of the nuclear levels, because of the recoil R to the nucleus. We can also see, that the recoil can be neglected for large nucleus mass m. In this experiment, we use solids which have a lattice structure. Therefore, the recoil does not only effect the nucleus but rather the whole lattice which has an even higher mass m. Thus, the recoil in this case is negligibly small.

What was not considered in the naive ansatz used above, is the excitation of the lattice. There are different models of the vibrational excitation of a lattice. The Einstein model for example describes the nuclei as non-coupled particles. Each nucleus moves in a harmonic potential and can take different excited states of a quantum mechanical harmonic oscillator. However, this model ignores the interactions between the nuclei and therefore fails at low energies, when the interaction of the nuclei is comparable to the thermal energy. This problem is fixed by the Debye model, where the nuclei are not treated independently. The lattice is rather described by a continuous solid. The excitations of the lattice are still quantized and the corresponding quanta are called phonons. Nevertheless, the Debye model is not able to explain every solid, but it is sufficient for the explanation of the Mößbauer effect.

As seen above, the kinetic recoil of the whole lattice is negligible. But there is still the possibility to pass the recoil energy to excitations of the lattice. This would also lead to a deviation of the photon energy from the energy difference of the nuclear levels. The probability to have an emission without lattice excitation is given by the Debye-Waller factor f. According to Ref. [8] the Debye-Waller factor f of the source can be calculated by:

$$f = \frac{\dot{N}(\infty) - \dot{N}(0)}{\dot{N}(\infty)} \cdot \frac{1}{1 - \exp(-T_A/2) J_0(iT_A/2)}, \tag{24}$$

where $\dot{N}(\infty)$ is the rate at infinity, $\dot{N}(0)$ the rate at the absorption peak, T_A the effective absorber thickness (which might be weighted for a split absorbtion spectrum) and J_0 the Bessel function of first kind and zeroth order.

3 Methods

3.1 Setup

The setup which is used for the Mößbauer spectroscopy will be described in the following. The setup mainly consists of the sample device with the radioactive sources and a sledge, on which the absorber materials are fixed, as well as the detection electronics.

3.1.1 Detection electronics

For the evaluation of the γ spectra a scintillator is used. When an incoming photon reaches the scintillator, it excites an electron onto a higher energy level. When this electron de-excites into the lowest possible state, a photon with the energy of the difference between the energy levels is emitted. This energy is typically smaller than the energy of the incoming photon. So depending on how much energy the incoming photon has, this process is repeated several times and a stream of emitted photons reaches the photo cathode at the end of the scintillator. There, an amount of electrons is released, which is proportional to the energy of the initial photon. Behind the scintillator, there is a photomultiplier (PM) which consists of multiple anodes at different high voltage levels. The electrons from the photo cathode are accelerated from anode to anode releasing more and more electrons. The number of electrons is multiplied. The avalenche of electrons is collected at the final anode and the current pulse is fed into a pre-amplifier (PA). The dependence between the voltage behind the PM and the energy of the incoming photon is to a good approximation linear.

In addition to the PA, a main amplifier (MA) is necessary. The MA allows an amplification with a variable gain and shaping time. The MA provides an uni- and a bipolar output. In this experiment, only the unipolar signal will be used and is, if necessary, split into further components of the electronical setup.

The amplified unipolar signal can be read out by a multichannel analyser (MCA). The MCA sorts the signal into channels depending on the height of its voltage and passes the number of counts per channel to a computer. Via the software “Genie 2000 Gammamessung und -analyse” the counts for each channel N in a time t are saved and can be used for further analysis of the spectrum.

Instead of the spectral evaluation of the signal, a timing single channel analyzer (TSCA) can be used. The TSCA has an upper and a lower energy limit. It takes the unipolar signal of the MA and gives a logical output, if the voltage of the signal is between the limits. Therefore, an energy window can be selected and used for only counting events in this energy range. There are two possible outputs of the TSCA – a positive and a negative one. Here only the positive output will be used. Additionally, the TSCA allows the set of a delay to the signal. This function is not necessary for this setup.

The signals of the amplifier and the TSCA can also be combined. This is helpful for adjusting the energy window of the TSCA. For this purpose, a linear gate is used. The linear gate takes the amplified signal as input and the logical signal from the TSCA as enable signal. The linear gate only gives an output of the amplified signal, if there is a logical signal from the TSCA at the same time. This means, that if the output signal is passed to the MCA, only the selected energy window will be read and can be observed in the software.

As the signal of the MA and the TSCA may be delayed, we use a delay unit, to match the signals. At the delay unit several delays can be added to the signal of the MA.

The output signal of the linear gate can also be connected to a counter which counts the number of signals arriving.

3.1.2 Sources and absorbers

Before starting the Mößbauer spectroscopy, it is necessary to calibrate the spectrum read out by the MCA, because the afore mentioned devices yield a spectrum not in units of energies, but channels. For this purpose, a calibration source can be used. The calibration source contains a primary source of ^{241}Am. In front of the primary, several x-ray fluorescent sources can be positioned. If they are excited by the primary source, they emit x-ray spectra with known peaks. The peaks can be used to connect the channels c to energies E.

Beside the calibration, before the measurement it is needed to investigate some underground and shielding effects. Firstly, the underground due to Compton scattering can be evaluated by shielding the emission of γ rays by aluminium plates of various thickness d. Secondly, the effect of the shielding by acrylic glass which is in front of the used absorber can be determined by using two acrylic glass plates of similar thickness.

For the Mößbauer spectroscopy, a ^{57}Co source is used. It is fixed on one end of the setup. We want to examine a stainless steel and a natural iron absorber. They can be placed on a sledge. This sledge is connected to a motor which moves the sample relative to the emission source of ^{57}Co. The sledge is controlled by a LabView program, where one can set the measurement time t and the sledge velocity v. The counts N during the measurement time are returned.

3.2 Experimental approach

First, we set up the electronics. For this purpose, the output of the different components are checked at an oscilloscope. The setup of the MA requires an amplification, which allows to observe the whole spectra used at the MCA. This means, that the amplification gain should be adjusted in a way that the highest calibration peak can still be observed, but as many channels as possible are in the range of the observed spectrum.

By using the MCA, it is now possible to perform calibration measurements. Therefore, we use the setup shown in Figure 4. The different calibration sources are positioned in front of the scintillator and the counts N per channel c are measured for a time t. With this setup, moreover the spectrum of the ^{57}Co source is measured without absorber.

Fig. 4: The setup for the spectral measurement with the MCA is shown.

For the further measurements, it is necessary to select the 14.4 keV peak of the ^{57}Co source, which can be done with the energy windows of the TSCA. To select the energy windows of the TSCA, the setup shown in Figure 5 is used. The TSCA is taken as enable signal for the amplified signal. First, we delay the amplified signal in a way that it occurs simultaneously to the TSCA signal. This is checked by using the oscilloscope again. If the delay is set up, we open the energy window completely. By observing the spectrum measured with the MCA, the limits can now be adjusted around the region we want to observe. When the energy windows are set, instead of the MCA the counter can be positioned behind the linear gate. The counter now only counts events which belong to the selected emission peak. This setup will be used for all further measurements.

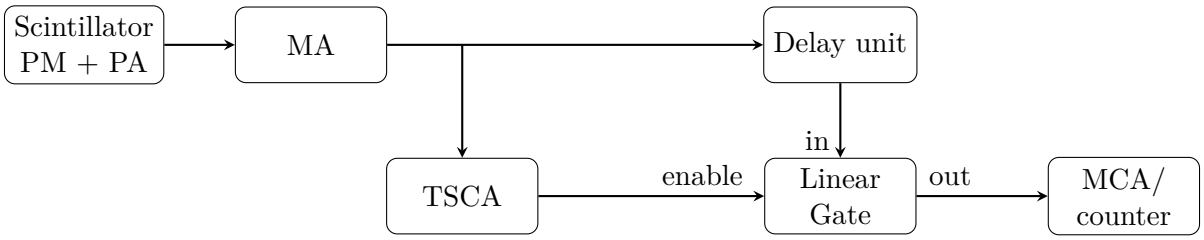

Fig. 5: The sketch shows the setup for adjusting the energy windows of the TSCA. The linear gate output can be passed to the MCA or a counter.

Before the Mößbauer spectroscopy starts, the background, originating from the Compton scattering of higher energetic photons, has to be determined. We position aluminium plates of thickness d in front of the scintillator. Now, the counts N in a time t are measured for different thicknesses d and the corresponding rate is calculated. Because the signal shielded by the aluminium plates depends on the energy of the shielded photon, the signal of the 14.4 keV peak is attenuated stronger than the signal of the high energetic photons leading to the Compton background. Both, the intensity of the Compton background and the signal, depend on the thickness d exponentially. The measured rates can be used to fit a double exponential to the data. This allows an extrapolation of the Compton background to the case without aluminium plates.

Moreover, the transmission T of the acrylic glass has to be determined. Therefore, we insert two plates of acrylic glass into the sample holder and measure the counts with and without acrylic glass.

As now all relevant background and shielding effects are quantified, the measurements of the absorbers can be performed. We measure the counts N for a time t at different sledge velocities v. By using the connection between velocity and energy resulting from the Doppler shift, these measurements give absorption spectra of stainless steel and natural iron.

4 Analysis and Results

4.1 Setup and signal shapes

Before starting the measurements, the NIM electronics need to be set up properly. This is done as described in Section 3.1.1. To check, if the setup is performed properly, the signal is observed on an oscilloscope at the most important points of the circuit. In Figure 6, screenshots of the oscilloscope are presented, showing the shapes of the signal at different points of the electronic setup.

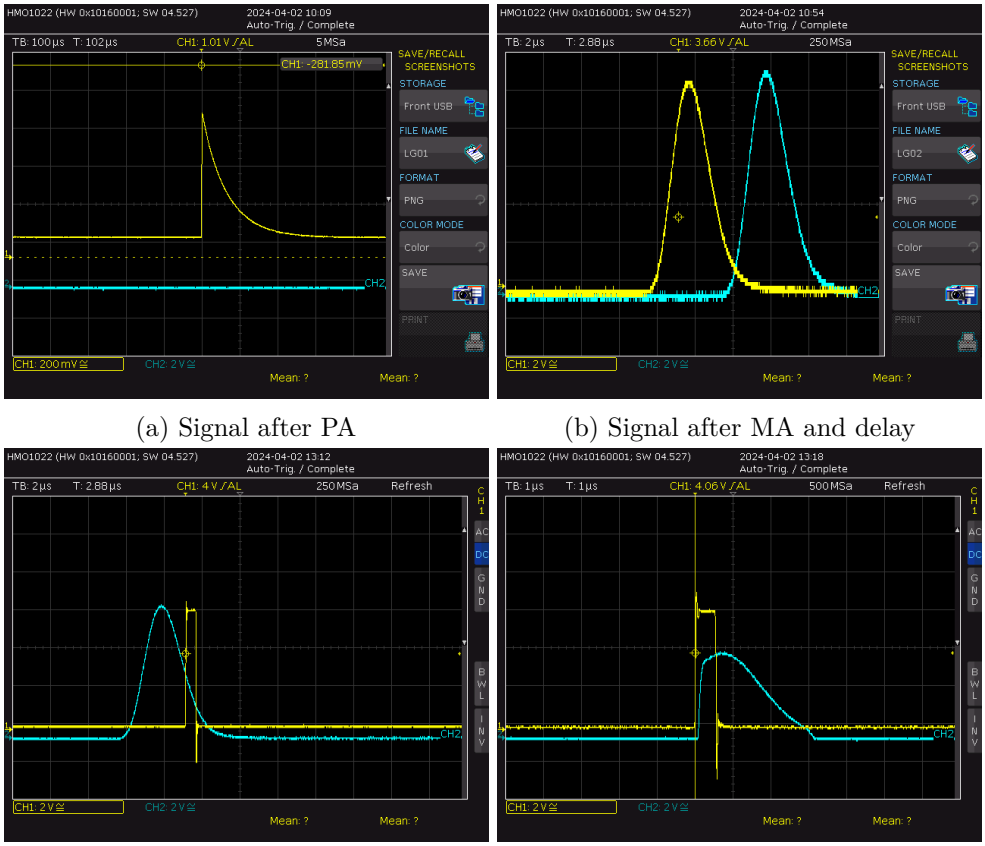

(a) Signal after PA

(b) Signal after MA and delay

(c) Signal after the TSCA

(d) Signal after the logical gate

Fig. 6: In the four pictures, different screenshots from the oscilloscope are presented, showing the signal at different points of the circuit. The signal in channel 1 is presented in yellow, and the signal coming from channel 2 in blue. The first picture shows the signal coming from the PA. In the second picture, the signal shape after the MA is shown, as well as a delayed version of the signal on channel 2. In the third picture, the same signal is shown on channel 2 and the output of the TSCA is presented on channel 1. The last picture, again shows the output of the TSCA, as well as the output of the logical gate in channel 2.

In Figure 6a, we see the signal coming directly from the PA of the photomultiplier. This signal has an exponentially decaying shape due to the discharge of the used capacitor. The signal is then directed to a MA, forming a Gaussian shape. The gain of the amplifier is set to a value, that the spectra of the calibration source fill the whole number of channels of the MCA. All chosen parameters can be found in Section 7.3 in the labnotes. In Figure 6b, this signal is shown, as well as the same signal with a delay of 4 µs added by a delay unit. In Figure 6c, in addition to the Gaussian shaped signal, a logical signal from the TSCA is shown, having a fixed height

and width. The TSCA only gives a logical signal, if the input signal has a certain height. This can be later used to set an energy window for the counter. With a logical gate, that is enabled by the logical signal of the TSCA, the signal is passed, if it has the desired energy. The output signal of this gate in portrayed in Figure 6d and can be passed to the MCA or the counter. Since all the signals have the desired form, the measurement can be started.

4.2 Calibration and window setup

After the setup of the electronics, the MCA can be used to measure emission or absorption spectra of radioactive sources. Since it only counts the rate of signals in arbitrary energy channels, to use the MCA properly, a calibration needs to be done. Therefore, the previously described calibration source can be used, providing five different absorbers with well known absorption energy. To get the channel number, we use a Gaussian distribution, that is fitted to the peak corresponding to the absorption with the known energy:

$$G(x; A, \mu, \sigma, y_0) = \frac{A}{\sqrt{2\pi}\sigma} \exp\left(-\frac{1}{2}\left(\frac{x-\mu}{\sigma}\right)^2\right) + y_0. \tag{25}$$

For the Tb absorber, in Figure 7, the measured spectrum is shown, as well as the performed fit using `scipy.optimize.curve_fit` [16]. The counts N are directly transformed into counting rates $\dot{N}$ by dividing by the measurement time t. For the uncertainty, we use the Poisson uncertainty $\Delta N = \sqrt{N}$, resulting in an error on the rates of $\Delta\dot{N} = \sqrt{N}/t$. For the other absorbers, comparable plots can be found in Figure 15 in the appendix.

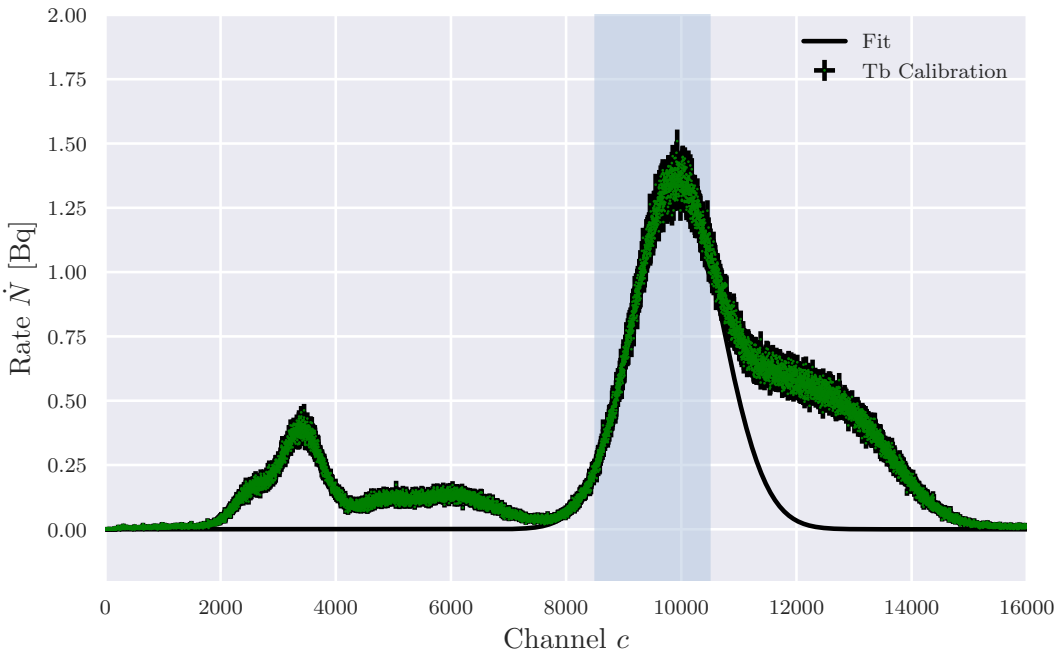

Fig. 7: In the graphic, the measured spectrum with the MCA of the Tb absorber is presented. The rate $\dot{N}$ in Bq $= s^{-1}$ is plotted against the arbitrary channel number c. The green data points are presented with black error bars. In addition, the fitted Gaussian is presented, with the fitting area marked in grey.

We then take the mean μ to assign a channel to the known absorption energy. As an uncertainty on μ, there are two possibilities. We can either take the fitting uncertainty, which is very small

and underestimates the uncertainty of the peak position or the standard deviation σ from the fit, which also accounts for uncertainties and noise coming from the physics and the electronics and is therefore preferred in the following analysis. A similar fit is performed for all the absorption sources. The values are presented in Table 1 together with the literature values of the energies taken from Ref. [17][1]. To get a measure of the quality of the fit, we use the reduced χ^2-value with the number of data points N, the measured values x_{exp}, the corresponding model values x_{mod} and the uncertainty Δx_{exp}:

$$\chi_0^2 = \sum_N \frac{(x_{\text{mod}} - x_{\text{exp}})^2}{\Delta x_{\text{exp}}^2}, \tag{26}$$

$$\chi^2 = \frac{\chi_0^2}{N - f}, \tag{27}$$

where f is the number of degrees of freedom. For a value of $\chi^2 \approx 1$, we can assume the model to be appropriate. Those values can also be found in the table.

Tab. 1: In the table, the fitted channel number c with uncertainty is given for every absorber, as well as the corresponding literature energy E in keV taken from Ref. [17]. In addition, a reduced χ^2 for the corresponding fit is added.

Calibration sample	energy E in keV	channel c	reduced χ^2
Tb	44.23	$10\,000 \pm 800$	1.0
Ba	32.06	7100 ± 600	1.3
Ag	22.10	5000 ± 500	1.2
Mo	17.44	4000 ± 400	1.1
Rb	13.37	3000 ± 400	1.1

We find that the reduced χ^2-value is approximately 1 for all the absorbers, justifying the choice of a Gaussian as a fitting function. Now, a linear regression can be performed, assigning every channel number to an energy value. Again, using `scipy.optimize.curve_fit` [16], we search for the fitting parameters a and b:

$$f(x) = a \cdot x + b. \tag{28}$$

The linear regression is presented in Figure 8. There, we do not include the uncertainty in the fit, since a better approximation of the calibration uncertainty is found using the uncertainty of the linear regression.

[1]The data could not be found in another source and is therefore taken from the instructions.

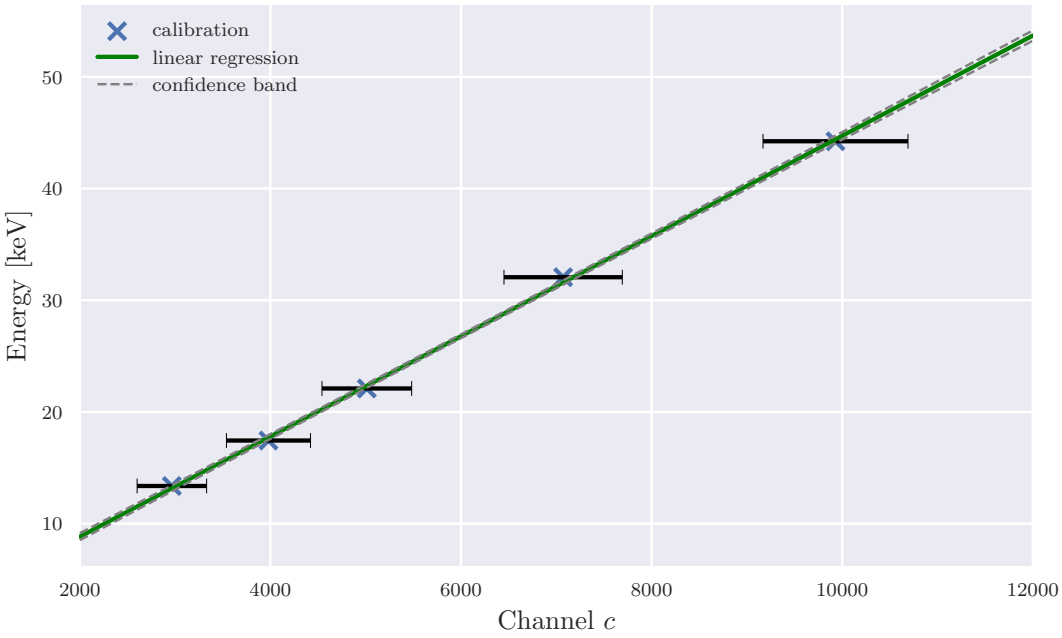

Fig. 8: In the plot, the calibration of the MCA can be found, with the known energy values from Ref. [17] in keV plotted against the channel number c in arbitrary units. In addition to the data with uncertainty, the linear regression is portrayed with a corresponding confidence band, which is however to small to be visible.

From the fit, we find the following calibration parameters:

$$a = (4.49 \pm 0.07)\,\text{eV}, \tag{29}$$

$$b = (-0.1 \pm 0.4)\,\text{keV}. \tag{30}$$

In general, we can say, that the uncertainties on the calibration are quite small, which can also be seen in the corresponding figure. This makes it possible to use the calibration reliably for the following measurement of the ^{57}Co source. Therefore, the channels can be directly converted using the following formula, with the uncertainty following from Gaussian error propagation:

$$E = a \cdot c + b, \tag{31}$$

$$\Delta E = \sqrt{(a\Delta c)^2 + (c\Delta a)^2 + (\Delta b)^2}. \tag{32}$$

We can now measure the spectrum of ^{57}Co and select a useful energy window around the peak to later only count events, resulting from the absorption and re-emission of this peak. To get an estimate for the size of the energy window, the expected width of the peak is needed. We therefore also perform a linear regression, plotting the standard deviation σ of the different calibration peaks against the energy, since the width also increases with energy. We then use the predicted value for approximately 14.41 keV to get an estimate for the width of the peak, since this is the expected energy. The linear regression for σ can be found in Figure 16 in the appendix and is again performed using `scipy.optimize.curve_fit` [16]. We then want to find the channel window Δc by taking 2σ at both sides of the peak. The approximate values for the width are:

$$1\sigma \approx 390, \tag{33}$$

$$\Rightarrow \Delta c \approx 1560. \tag{34}$$

In the software, a window of approximately this size is marked and with the TSCA, a window is selected that approximately matches the marked range. In Figure 9, the spectrum is plotted with and without the set energy window. Due to very low counting rates, the peak is only visible after a fairly long measurement time of more than an hour. This point will be discussed later in the final part of the report.

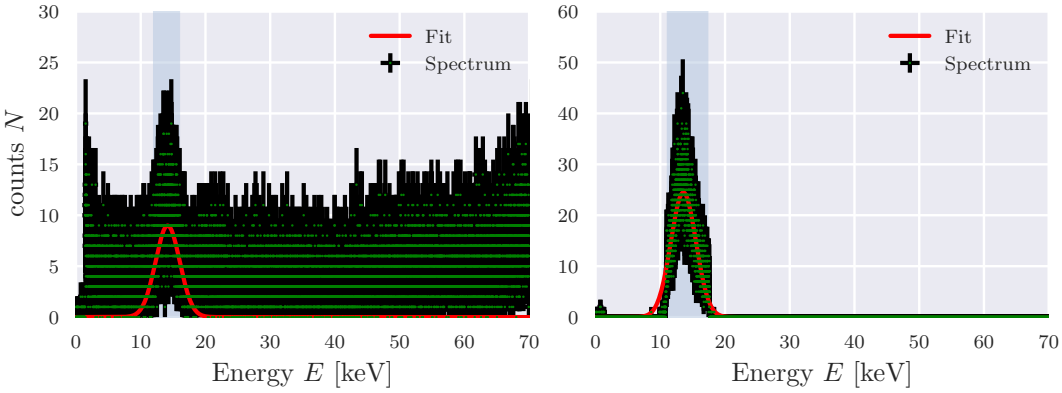

Fig. 9: In the graphics, the spectrum of the ^{57}Co are presented, both measured for more than an hour. For both spectra, the number of counts N is plotted against the energy E in keV. In the left graphic, the total spectrum is presented, whereas in the right graphic, the measurement after the window setup is shown. In red, a fit to the expected peak is added.

Using `scipy.optimize.curve_fit` [16], again, a Gaussian distribution is fitted to the visible peak. By doing so, we can check, whether the right peak position is selected or not. In Table 2, the fitted energies are presented, with the uncertainty on the energy coming again from the standard deviation σ. In addition, a reduced χ^2-value is added as well as a t-value, which corresponds to the deviation from the literature value of $(14.412\,95 \pm 0.000\,31)$ keV [18] divided by the uncertainty.

Tab. 2: The table summarizes the fitted peak energies E for both, the total spectrum and the spectrum cut off by the energy window. In addition, a reduced χ^2-value and a t-value for the comparison with literature is added.

	peakenergy E in keV	reduced χ^2	t-values
complete spectrum	14.2 ± 1.9	1.1	0.13
selected peak	13.6 ± 1.9	1.1	0.44

We see that for both values, we find a good compatibility with literature in range of the uncertainties, which confirms, that the desired peak actually matches the chosen energy window. In addition, the reduced χ^2-values of approximately 1 indicate a good choice of the Gaussian fitting function.

4.3 Sledge velocity

For the later measurements of the absorption spectra, a very accurate sledge velocity is essential. Because we want to perform a high precision measurement using the Doppler effect, a study of the

sledge velocity is added to ensure its trustworthiness. We therefore perform two measurements of the sledge velocity. First, we take 10 measurements of a velocity setup of $5\,\mathrm{mm\,s^{-1}}$. Taking several measurements reduces the statistical uncertainty. The velocity v is measured, by marking a distance of $d = (80.0 \pm 0.4)\,\mathrm{mm}$ and stopping the passing time t using a stop watch. Here, an uncertainty of 0.3 s is estimated, since it is not completely sure, when the sledge passes the marked positions. Calculating the velocities $v = \frac{s}{t}$ and taking the mean we find:

$$v = (5.01 \pm 0.03)\,, \tag{35}$$

$$t = 0.19. \tag{36}$$

The t-value shows a good compatibility with the set up velocity of $5\,\mathrm{mm\,s^{-1}}$. To also check, whether there is an offset in the sledge velocities and control, that the whole range of velocities is properly working, we also measure several velocities, ranging from $1\,\mathrm{mm\,s^{-1}}$ to $10\,\mathrm{mm\,s^{-1}}$. The velocities are calculated in the same way as before. In Figure 10, the measured data is presented, as well as a performed linear regression.

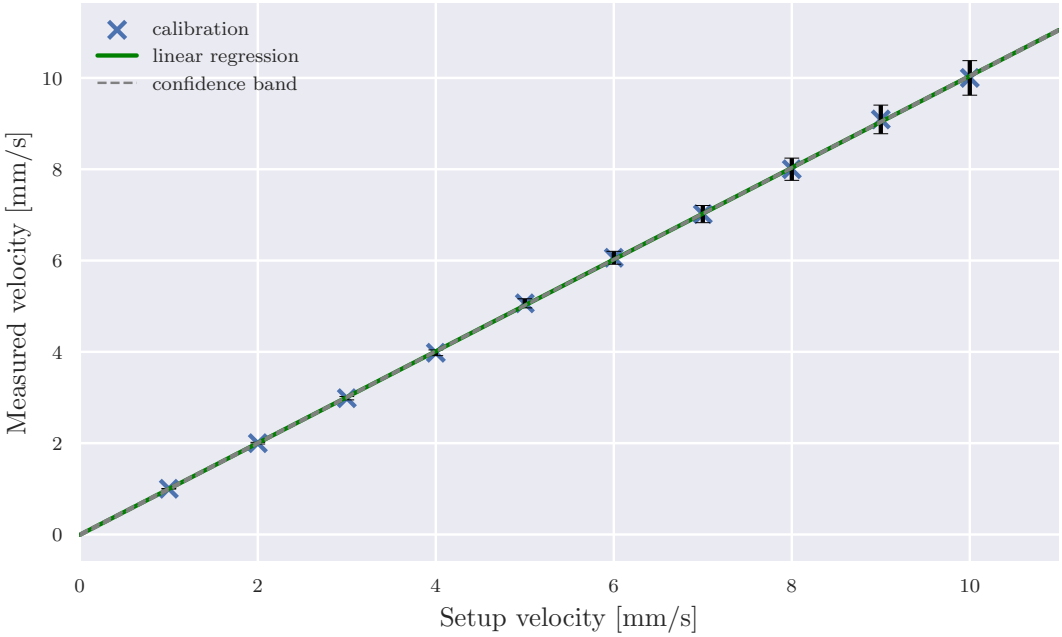

Fig. 10: In the plot, the measured velocities are plotted against the set up velocities in the software, both in $\mathrm{mm\,s^{-1}}$. In addition, a linear regression is added with confidence band, which is however not clearly visible.

From the linear regression, we find the following values for the slope a and the y-intercept b:

$$a = 1.005 \pm 0.004, \tag{37}$$

$$b = (-0.01 \pm 0.03)\,\mathrm{mm\,s^{-1}}. \tag{38}$$

Those values are in good agreement with a model, where the measured velocity is equal to the one set in the software. For this model, we would expect an intercept of $b = 0\,\mathrm{mm\,s^{-1}}$ and a slope of $a = 1$. In the following, one could use the measured values for a calibration of the velocities. However, since the previous results also show good agreement with the assumption, that the software setup is optimal, the inaccurate measurement technique with a stop watch can also lead to a non-improvement of the values and only adds uncertainty to the data. In the following, we therefore always use the sledge velocity given by the software.

4.4 Background considerations

Before starting the measurements of the different absorbers, additional considerations on the background need to be performed. More precisely, we want to identify sources influencing the counting rate, so that we can later correct the measurement data. In the following, two main effects are studied. Firstly, as already explained in the theory part, there is Compton scattering in the scintillator due to higher energy transitions. In the scintillator, this scattering can lead to additional counts in the selected energy window. The second effect is an attenuation of the signal by the acrylic glass plates around the given samples. In contrast to the Compton background, this damps the signal and therefore a correction increasing the signal needs to be used.

4.4.1 Compton background

For the measurement of the Compton background, we use the following approach: Several aluminium plates are brought between the scintillator and the source. The measurement is performed without the acrylic glass, which later needs to be considered when calculating the correction of the rate. We observe differently strong damping for the signal and the Compton background as explained in the methods part. While the signal is damped very strongly, we only have small damping of the Compton background. We can therefore perform a fit using a sum of two exponential decay functions representing the different damping strengths:

$$f(x) = A\exp(ax) + B\exp(bx). \tag{39}$$

We take data for aluminium thicknesses d between 0 mm and 10 mm, which is shown in Figure 11 together with the respective fits performed with `scipy.optimize.curve_fit` [16]. In addition to the double exponential, the long ranging part accounting for the Compton background is plotted.

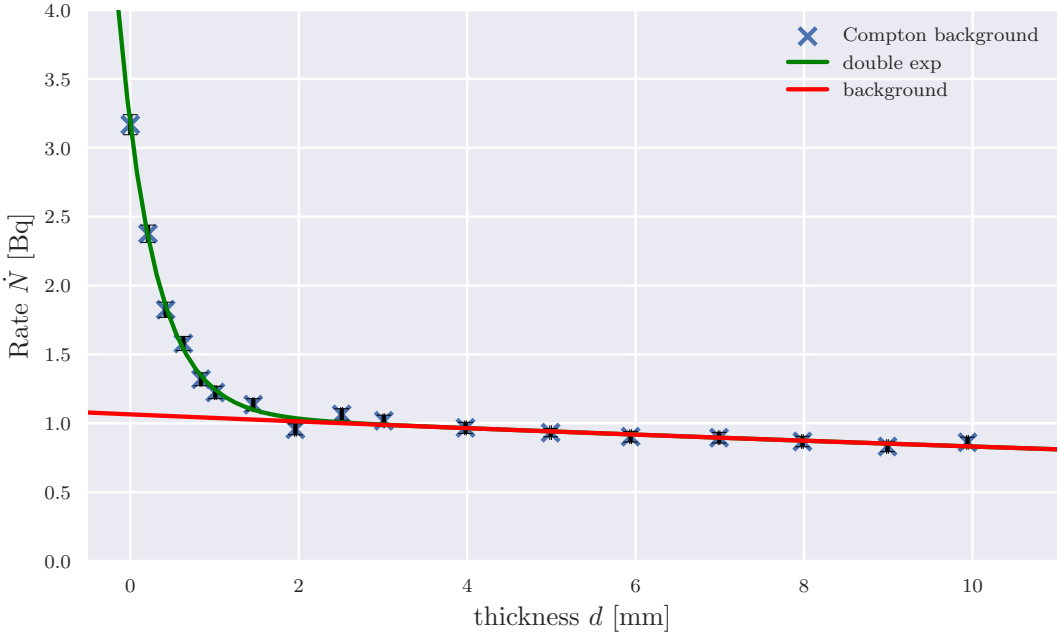

Fig. 11: In the graphic, the measured rate $\dot{N}$ in Bq = s^{-1} with uncertainty is plotted against the thickness d of the used aluminium plates. In addition, the fit using a double exponential is added in green. In red, one can see the corresponding exponential decay, only accounting for the Compton background.

For the fit, we find $\chi^2 = 0.7$, which confirms the assumption of two overlaying exponential decays. Since for later measurements, we do not use aluminium plates, for the Compton background, we use an extrapolation of the corresponding Compton exponential to zero thickness. Therefore, we can directly use the fitting parameter B as the rate correction $\dot{N}_C$. Using the fitting uncertainty, we find the following parameters:

$$A = (2.11 \pm 0.04)\,\mathrm{Bq}, \tag{40}$$
$$a = -2.316 \pm 0.019, \tag{41}$$
$$B = (1.06 \pm 0.03)\,\mathrm{Bq} = \dot{N}_C, \tag{42}$$
$$b = -0.025 \pm 0.010. \tag{43}$$

4.4.2 Acrylic glass damping

An additional correction factor comes from the attenuation through the acrylic glass. We can take this into account by comparing the rate measured with and without an acrylic glass absorber to find a transmission T. However, the two rates also need to be corrected with the Compton background measurement leading to:

$$T = \frac{\dot{N}_A - \dot{N}_C}{\dot{N}_0 - \dot{N}_C}, \tag{44}$$
$$\Delta T = \frac{1}{\dot{N}_0 - \dot{N}_C}\sqrt{\left(\Delta\dot{N}_A\right)^2 + \left(T\Delta\dot{N}_0\right)^2 + \left(\frac{\dot{N}_A + \dot{N}_0 - 2\dot{N}_C}{\dot{N}_0 - \dot{N}_C}\Delta\dot{N}_C\right)^2}. \tag{45}$$

With a measuring time of 600 s, we find the following uncorrected rates with acrylic glass $\dot{N}_A$ and without acrylic glass $\dot{N}_0$:

$$\dot{N}_A = (2.53 \pm 0.06)\,\mathrm{Bq}, \tag{46}$$
$$\dot{N}_0 = (3.17 \pm 0.07)\,\mathrm{Bq}. \tag{47}$$

Those values can be combined to:

$$T = 0.70 \pm 0.05. \tag{48}$$

In addition, the transmission factor can be calculated theoretically using Equation 19. We therefore use values for the absorption coefficient $\frac{\mu}{\rho} = (1.1 \pm 0.3)\,\mathrm{cm^2\,g^{-1}}$ and the density $\rho = (1.1 \pm 0.3)\,\mathrm{g\,cm^{-3}}$ taken from [17][2], as well as the thickness of the acrylic glass which is measured to be $d = (0.196 \pm 0.002)\,\mathrm{cm}$. Inserting these values into the formula results in

$$T_{\mathrm{theo}} = (0.77 \pm 0.05) \tag{49}$$

Comparing the experimentally and theoretically found values, we find a t-value of $t = 1.1$, showing that both values are comparable. However, for the following analysis, we will take the measured value, since this value is not based on values given in the experiment instructions, and therefore might be more suitable for our used setup. For every measured rate $\dot{N}_0$, we can now find the corrected rate by

$$\dot{N} = \frac{\dot{N}_0}{T} - \dot{N}_C, \tag{50}$$
$$\Delta\dot{N} = \sqrt{\left(\frac{\Delta\dot{N}_0}{T}\right)^2 + \left(\dot{N}\Delta T\right)^2 + \left(\Delta\dot{N}_C\right)^2}. \tag{51}$$

It is hereby important to note, that the transmission is only used to correct the measured rate and not the Compton background, since the background was measured without acrylic glass.

[2]The data could not be found in another source and is therefore taken from the instructions.

4.5 Stainless steel absorber

The first sample to be investigated is the stainless steel absorber. Here, a single peak is expected showing an isomeric shift. It is therefore sufficient to measure with sledge velocities between $-2\,\mathrm{mm\,s^{-1}}$ and $2\,\mathrm{mm\,s^{-1}}$. Around the peak, steps of $0.05\,\mathrm{mm\,s^{-1}}$ are taken, whereas for the higher velocities, only steps of $2\,\mathrm{mm\,s^{-1}}$ are chosen. To minimise the uncertainties, we strive for a long measurement time. In total, the data is taken for 23.5 h, which is the pure measurement time summed up for all data points.

There are three possible models, that can be used to describe different aspects of the absorption peak. Due to high noise on the data, one possible model would be a Gaussian function G for the fit, which accounts for fluctuations in the absorption and Doppler broadening, as well as for noise from the electronics. A model accounting for the physics of the absorption peak would be the Lorentz profile L. Since often the expected Lorentz peak is overlayed by noise to a certain extend, a mixture of both models can also be used. The so-called Voigt function V is a convolution of a Gaussian function with a Lorentz function, and can therefore be used to extract the different contributions to the peak. We use

$$G(x; A, \mu, \sigma, y_0) = -\frac{A}{\sqrt{2\pi}\sigma} \exp\left(-\frac{1}{2}\left(\frac{x-\mu}{\sigma}\right)^2\right) + y_0 \tag{52}$$

$$L(x; A, \mu, \gamma, y_0) = -\frac{A}{\pi}\frac{\gamma}{(x-\mu)^2+\gamma^2} + y_0, \tag{53}$$

$$V(x; A, \mu, \sigma, \gamma, y_0) = -A \cdot (G \star L)(x; \mu, \sigma, \gamma) + y_0, \tag{54}$$

as fitting functions, with mean μ, width parameters σ and γ, proportionality constant A and y-intercept y_0.

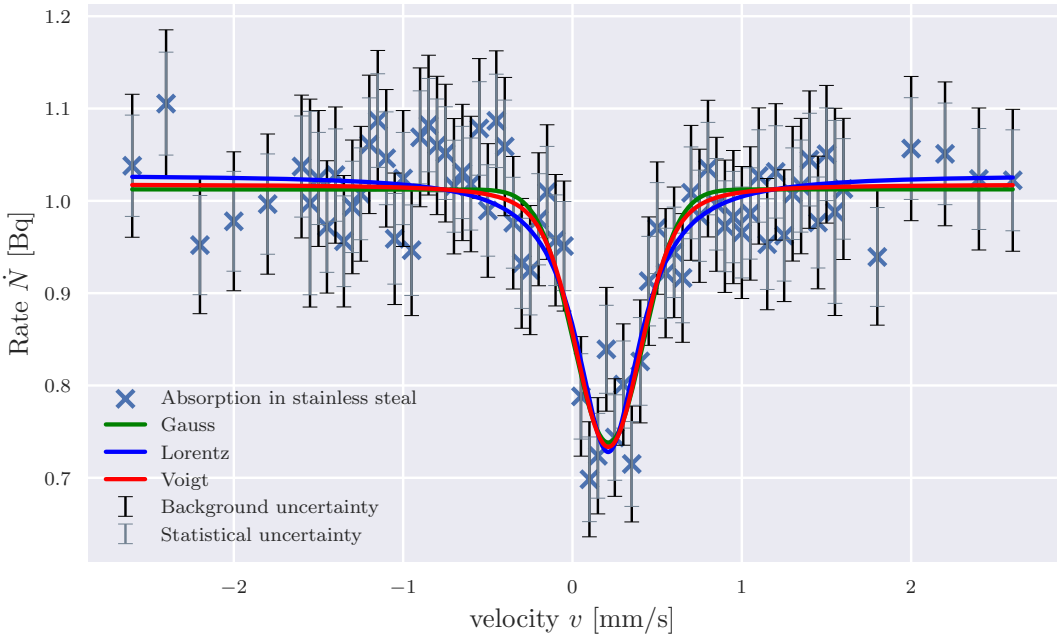

Fig. 12: The measured data points for the absorption in stainless steel are presented together with the corresponding error bars. The rate $\dot{N}$ in Bq = $\mathrm{s^{-1}}$ is plotted against the sledge velocity v in $\mathrm{mm\,s^{-1}}$. In addition, using three different colours, the fits for the three different models are presented. Statistical and background uncertainties are plotted in different colours.

The measured data is presented in Figure 12 and fits for all three models are added. Again, to fit the data, we use `scipy.optimize.curve_fit` [16] with the uncertainties of the data points taken into account. Looking at the plot one can directly see, that all three fits describe the data in a similar way, having compatible amplitudes and peak positions, as well as y-intercepts. One can also observe, that the Voigt function is indeed a compromise between Gaussian and Lorentz function, with the curve lying in the middle of the other ones. Similar conclusions can be found, when looking at the fitting parameters summarized in Table 3. There, the reduced χ^2-values are also presented, which are all smaller than one, showing that the data is well described by the fits, but the uncertainties of the data are extremely high and mainly dominated by the statistical uncertainties and not the background considerations. If one looks at the residuals, one can also see that only few data points are not in a 1σ range of the fits, leading to this low value of the reduced χ^2. The residual plots can be found in Figure 17 in the appendix. This will also be part of the discussion.

Tab. 3: In the table, all fitting parameters of the three models for the fits for stainless steel are summarised with the corresponding fitting uncertainty. The reduced χ^2-value is also added for every fit.

Function	μ in mm s^{-1}	σ in mm s^{-1}	γ in mm s^{-1}	A in Bq	y_0 in Bq	reduced χ^2
Gauß	0.21 ± 0.03	0.21 ± 0.03	-	0.14 ± 0.02	1.012 ± 0.010	0.4
Lorentz	0.21 ± 0.03	-	0.23 ± 0.05	0.22 ± 0.04	1.028 ± 0.013	0.4
Voigt	0.21 ± 0.03	0.16 ± 0.12	0.09 ± 0.18	0.17 ± 0.06	1.018 ± 0.015	0.4

Also from the fitting parameters, we find similar results for μ and y_0. The differences in A result from the fact, that all models have a different relation between height and normalisation, which means that for similar shapes, A could still differ. We also find, that the Voigt fit has both, Gaussian and Lorentz parts determined by the strength of σ and γ, but the errors on both parameters are very high. This may come from the fact, that both, Gaussian and Lorentz curves describe the data quite well and therefore any model between Lorentz and Gauß would so too. Therefore, we have very high uncertainties on the parameters determining how strongly one of the models dominates in the Voigt function. This argument is also supported by a strong anti-correlation of $\rho = -0.95$ between σ and γ, indicating, that increasing the influence of one of the two models is always connected to a decrease of the influence of the other model.

In the following, the found fitting parameters can be used to evaluate different properties of the stainless steel absorber.

4.5.1 Isomeric shift

In a first step, we can find the isomeric shift of the absorber. As explained in the theory, this property describes an energy deviation from the emission of the ^{57}Co source. In the data, the isomeric shift is found as a displacement of the peak position from zero velocity. Using the Doppler effect, the isomeric shift can easily be computed from the velocity deviation v from zero

$$E_{\text{iso}} = E_0 \frac{v}{c}, \tag{55}$$

where the energy of the emission peak $E_0 = (14.412\,95 \pm 0.000\,31)\,\text{keV}$ [18] is taken as the reference energy. Using the fitting parameters for the mean μ for all three models and using

Gaussian error propagation for the uncertainties we find:

$$E_{\text{iso},G} = (10.2 \pm 1.4)\,\text{neV}, \tag{56}$$
$$E_{\text{iso},L} = (10.1 \pm 1.3)\,\text{neV}, \tag{57}$$
$$E_{\text{iso},V} = (10.2 \pm 1.3)\,\text{neV}. \tag{58}$$

All the values are very good compatible with each other, which is not surprising, since already the peak positions were very similar. A comparison to literature values is not possible, since no values are known, however, all the values show the correct order of magnitude of several neV.

4.5.2 Effective thickness

As introduced in the theory part, the effective absorbed thickness T_A is a measure of interactions in the absorber and can be calculated using several material properties:

$$T_A = f_A n_A \beta \sigma d. \tag{59}$$

Whereas σ and n_A need to be calculated separately, all the other values can be found in literature. For σ, Equation 9 is used, as introduced in the theory. For the number density n_A we use

$$n_A = \rho \frac{N_A}{M} p, \tag{60}$$
$$\Delta n_A = \rho \frac{N_A}{M} \sqrt{(\Delta p)^2 + \left(\frac{p}{M}\Delta M\right)^2}. \tag{61}$$

with the density ρ, the molar mass M, the Avogadro constant N_A and the fraction of iron in the absorber p. The uncertainty is calculated using Gaussian error propagation. The recoilless emission probability $f_A = 0.8$, the sample thickness $d_A = 25\,\mu\text{m}$, the isotope fraction $\beta = 0.022$ and the iron content fraction $p = (70 \pm 5)\,\%$ are all provided in the experiment instructions [17][3], the molar mass $M = (55.845 \pm 0.002)\,\text{g mol}^{-1}$ and the density $\rho = 7.874\,\text{g cm}^{-3}$ are taken from an external source [13] and the conversion coefficient $\alpha = 8.58 \pm 0.18$ needed for the calculation of the cross section σ is taken from Ref. [18]. Plugging in all the values and using Gaussian error propagation we find:

$$n_A = (0.099 \pm 0.007)\,\text{mol cm}^{-3}, \tag{62}$$
$$\sigma = (2.46 \pm 0.05)\,\text{Mb}, \tag{63}$$
$$\Rightarrow T_A = 6.4 \pm 0.5. \tag{64}$$

This factor cannot be compared to literature again. Its uncertainty does not result from measurements, but rather from the high uncertainty of the iron content and can therefore not be reduced.

4.5.3 Debye-Waller factor

In a next step, the probability to have an emission in the source without a lattice excitation needs to be evaluated. This is done by calculating the Debye-Waller factor f_Q as introduced in the theory part. Redefining some variables and using error propagation we find:

$$f_Q = \frac{\dot{N}(\infty) - \dot{N}(\mu)}{\dot{N}(\infty)(1 - \exp(-T_A/2)J_0(iT_A/2))} = \frac{A}{B(1 - \exp(-T_A/2)J_0(iT_A/2))}, \tag{65}$$
$$\Delta f_Q = \sqrt{\left(\frac{f_Q}{A}\Delta A\right)^2 + \left(\frac{f_Q}{B}\Delta B\right)^2 + \left(\frac{A\exp(T_A/2)\left(J_0(iT_A/2) + iJ_1(iT_A/2)\right)}{2B\left(\exp(T_A/2) - J_0(iT_A/2)\right)^2}\Delta T_A\right)^2}. \tag{66}$$

[3]The data could not be found in another source and is therefore taken from the instructions.

For the rate at infinite energy B, we use the plateau value of the spectrum given by the fitting parameter for the y-intercept y_0. For the difference between minimal and maximal rate A, however, we cannot use a single parameter, since the normalisation parameter in the fit scales differently for different models. Instead, the rate at the peak position $\dot{N}(\mu)$ is taken and the difference to the y-intercept is calculated. Finding those two values for all three models and using the effective absorber thickness calculated in the previous section, we find:

$$f_{Q,G} = 0.354 \pm 0.015, \tag{67}$$
$$f_{Q,L} = 0.381 \pm 0.015, \tag{68}$$
$$f_{Q,V} = 0.36 \pm 0.02. \tag{69}$$

The three values are again compatible with each other, but show higher deviations as the isomeric shift. This may be due to the fact, that the fits for all three models have nearly excactly the same peak position, but show larger deviations in amplitude and y-intercept. Literature values can again not be provided, but a rate of $\approx 35\,\%$ can be reasonable for the percentage of recoilless emissions.

4.5.4 Linewidth and lifetime

As explained in the theory, the lifetime τ of the state can directly be obtained by the full-width-half-maximum (FWHM) value Γ of the corresponding peak using $\tau = \hbar/\Gamma$. For the calculation of the lifetime, we therefore first need to find an expression for the FWHM of all three models.

$$\Gamma_G = 2\sqrt{2\ln(2)}\sigma, \tag{70}$$
$$\Gamma_L = 2\gamma, \tag{71}$$
$$\Gamma_V = 0.5346\gamma + \sqrt{0.2166\gamma^2 + \sigma^2}. \tag{72}$$

It is important to notice, that for the Gauß and Lorentz models, those formulas are exact and can be found analytically, whereas for the Voigt function, the equation is an approximation, exact only within a relative uncertainty of $0.023\,\%$ [19]. In addition, one goal of the use of Voigt function is to extract the Lorentz part from the convolution with a Gaussian. It might therefore also be interesting, to extract this part and use the Lorentz FWHM $\Gamma_V = \Gamma_L = 2\gamma$ instead of the approximation formula. This however, sometimes causes problems due to the fact, that in our measurement with high statistical uncertainties the Voigt function does not describe the mixture of Gaussian and Lorentz functions reliably as will be seen later and discussed in the final part of the report.

In addition, when not only measuring the spectrum of an emitter, but rather the absorbed spectrum of emitted radiation, relative-broadening corrections need to be taken into account. Already for emitter and absorber of infinitesimal small size, the FWHM is doubled due to re-emission after absorption, leading to a fraction of $\frac{\Gamma}{\Gamma_0} = 2$. For effective source and absorber thicknesses larger than zero however, we get additional broadening. We therefore also need to find the effective source thickness T_Q, which is calculated in a similar way:

$$T_Q = f_Q n_Q \beta \sigma_0 d_Q \tag{73}$$

For f_Q, the Debye-Waller factor is taken from above. We assume $n_Q \approx n_A$, $\beta = 1$, and $d_Q \approx 100\,\text{Å}$ as described in the instructions to the experiment [17] and the other variables do not change and are therefore taken from above. We find

$$T_{Q,G} = 0.052 \pm 0.002, \tag{74}$$
$$T_{Q,L} = 0.056 \pm 0.003, \tag{75}$$
$$T_{Q,V} = 0.053 \pm 0.003, \tag{76}$$

justifying the assumption, that the source thickness is negligible, especially in comparison to the absorber thickness. Therefore we can use Equation 7 [7] to find a correction factor on the FWHM for all the models. Inserting the effective absorber thickness T_A, which is equal for all three models we find

$$\frac{\Gamma}{\Gamma_0} = 3.68 \pm 0.11, \tag{77}$$

which can now be used as a correction on the FWHM. We now have all tools to calculate the lifetime of the state corresponding to the measured peak. In Table 4, the values for the non-corrected and corrected FWHM are summarised for all three models, as well as the corresponding lifetimes τ, also calculated for the corrected and non-corrected values. In addition, a t-value is calculated for the comparison of the corrected lifetime with the literature value of $\tau_{\text{lit}} = 141\,\text{ns}$ [20].

Tab. 4: In the table, for all three models, the corrected and non-corrected FWHM values in neV are summarized, together with the corresponding lifetimes τ in ns. In addition, a t-value is calculated, comparing the corrected lifetime with the literature value taken from Ref. [20]. For the Voigt function, both approaches using only the Lorentz FWHM and the approximation formula are presented.

Function	FWHM Γ [neV]	Lifetime τ [ns]	corr. FWHM Γ_0 [neV]	corr. Lifetime τ_0 [ns]	t-value
Gauß	23 ± 3	28 ± 4	6.6 ± 0.9	104 ± 15	2.4
Lorentz	22 ± 5	30 ± 6	6.0 ± 1.3	110 ± 20	1.2
Voigt, Lorentz FWHM	9 ± 17	80 ± 150	2 ± 5	300 ± 600	0.3
Voigt, Voigt FWHM	20 ± 40	30 ± 50	60 ± 100	110 ± 170	0.19

There are several conspicuous points that need to be mentioned, when looking at the values. First of all, we can see that the non-corrected lifetimes underestimate the real lifetime by a very large factor. In comparison, the corrected lifetimes are a lot closer to the actual value. This justifies the use of the correction considering the effective absorber thickness. As a second remark, if one looks at the uncertainties, one can see that for the Lorentz and Gauß they are significantly smaller than for the Voigt model. For those models, the relative uncertainty is still larger than 10 %, this can be explained by the high uncertainties on the data due to small counting rates. For the Voigt model however, the high uncertainties result again from the high uncertainties on the width parameters, which can be explained by the fact, that both, a Gaussian and Lorentz shape are good estimates for the data. Therefore in the Voigt function, the width parameters can more or less be split arbitrarily between the two models. In addition, this also leads to the observation, that using the Lorentz FWHM, the value deviates by a large amount and has an uncertainty of approximately twice the value. All of these points will again be thematised in the discussion part.

A visualisation of the linewidth correction can be found in Figure 13. Here, in addition to the original Lorentz fit to the data, the Lorentz function corresponding to a corrected FWHM is shown, as well as the theoretical prediction, when taking the literature lifetime τ_{lit}. One can see, that the corrected linewidth is a lot closer to the actual line width predicted by the literature value.

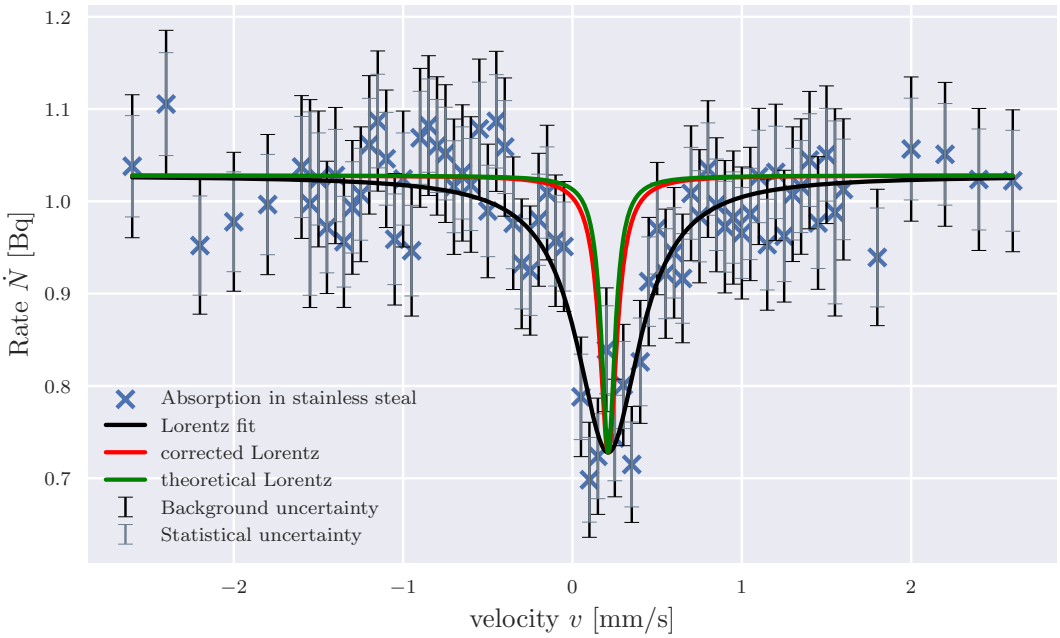

Fig. 13: In the graphic, a visualisation of the lifetime correction in provided. In addition to the absorption spectrum of stainless steel and the corresponding Lorentz fit, the Lorentz curve, one would find for the corrected linewidth is shown in red, as well as the theoretical prediction from the literature value τ_{lit} in green. Again, the rate $\dot{N}$ in $\text{Bq} = \text{s}^{-1}$ is plotted against the sledge velocity v in $\text{mm}\,\text{s}^{-1}$. Statistical and background uncertainties are plotted in different colours.

4.6 Natural iron absorber

Similar considerations can now be performed for the natural iron absorber, where we expect, in addition to the isomeric shift, a hyperfine splitting into six different absorption peaks. For the measurement, the same setup is taken as for the stainless steel absorber, but a longer measurement time of 57.2 h in total is achieved. This is due to the fact, that a significantly larger velocity range needs to be scanned in order to observe the complete hyperfine spectrum. In a range from $-7\,\mathrm{mm\,s^{-1}}$ to $7\,\mathrm{mm\,s^{-1}}$, steps of $0.1\,\mathrm{mm\,s^{-1}}$ are chosen for the data points. The rates $\dot{N}$ are again corrected with the Compton background and the transmission of the acrylic glass.

As explained before in the theory part, due to internal magnetic fields, we expect a hyperfine splitting in the spectrum. We therefore need to adjust the fitting functions to sums of six Gauß, Lorentz or Voigt profiles with a common intercept y_0. In Figure 14, the absorption spectrum in natural iron is presented together with the fits performed using `scipy.optimize.curve_fit` [16]. The corresponding fitting parameters as well as reduced χ^2 values can be found in tables in the appendix, with the parameters for the Gauß profile in Table 9, of the Lorentz profile in Table 10 and of the Voigt profile in Table 11. Again, residual plots can be found in Figure 18 in the appendix.

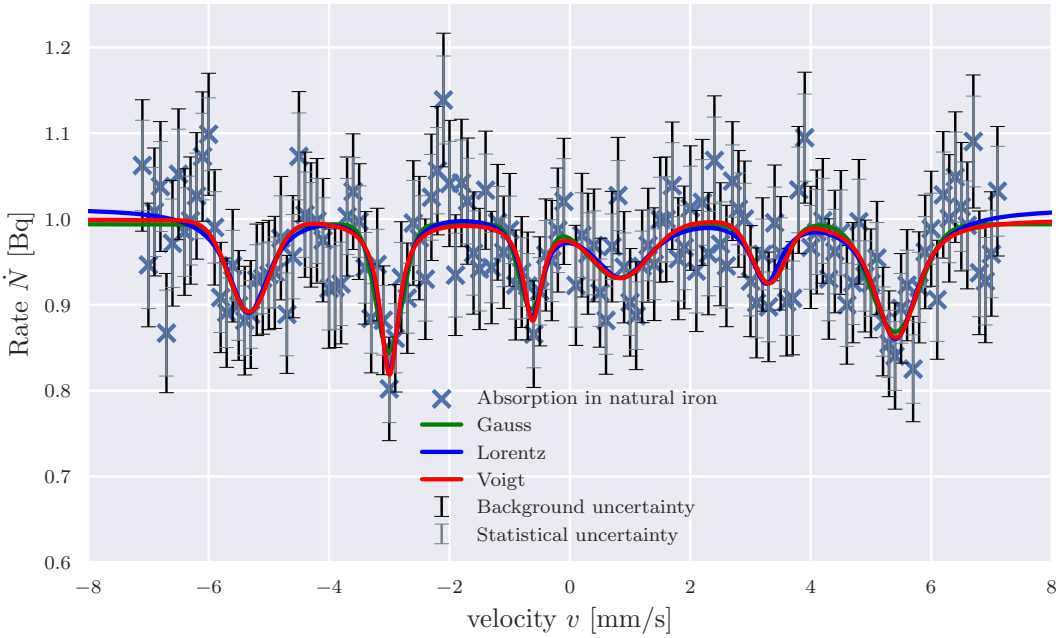

Fig. 14: The measured data points for the absorption in natural iron are presented together with the corresponding error bars. The rate $\dot{N}$ in $\mathrm{Bq} = \mathrm{s^{-1}}$ is plotted against the sledge velocity v in $\mathrm{mm\,s^{-1}}$. In addition, using three different colours, the fits for the three different models are presented, with every model being a sum of six individual peak profiles.

As for the stainless steel absorber, we have very small reduced χ^2-values of approximately 0.5 for all three models, again being an artifact of the high uncertainties on the counting rates due to low intensity of the source. The uncertainties are also dominated by statistical uncertainty on the counts. As previously, all three models show similar fitting parameters for the intercept y_0 and the peaks positions μ, as well as for the normalisations A, when accounting for the different scaling for the three models.

In contrast to the previous absorber, the Voigt fit now only has non-vanishing values for both σ and γ for the third peak on the right. For all other peaks, one of the two values is vanishing completely, reducing the Voigt fit to a fit of one of the other models. However, again, the uncertainties on both γ and σ are very high, being a lot larger than the value itself for all peaks. This indicates, that the given data is not sufficient to be clearly assigned to a specific model, but rather is very good compatible with both Lorentz and Gauß model and therefore also with any model containing both properties.

4.6.1 Isomeric shift and hyperfine structure

For the second absorber, we also expect an isomeric shift on all of the peaks. In this case it can, however, not be computed by simply taking the peak position and its deviation from zero. Instead, the isomeric shift is defined by the shift of the axis around which the peaks are arranged symmetrically. For one peak on the left and its counterpart on the right we therefore use

$$E_{\text{iso}} = \frac{|E_{i,\text{left}}| - |E_{i,\text{right}}|}{2}, \tag{78}$$

to find the isomeric shift. The energies can be calculated from the means of the different fits and converted from velocities to energies, using the Doppler shift as introduced in Equation 55. Again, Gaussian error propagation is used to compute the uncertainties. This leads to three values per model which can be averaged to get an estimate for the isomeric shift. As an uncertainty, the standard deviation of the mean is taken. The following values are found:

$$E_{\text{iso},G} = (4.3 \pm 1.4)\,\text{neV}, \tag{79}$$
$$E_{\text{iso},L} = (4.5 \pm 1.1)\,\text{neV}, \tag{80}$$
$$E_{\text{iso},V} = (4.9 \pm 1.3)\,\text{neV}. \tag{81}$$

The values are all compatible with each other and have the right order of magnitude. Again, no literature value is known for comparison.

In addition to the isomeric shift, the hyperfine structure of the sample is detected. The deviations from the symmetry axis correspond to the deviations from the expected energy transition as decribed in the theory part. They can be computed, by correcting the peaks with the isomeric shift and averaging between the values of the left and the corresponding right peak energy:

$$E_i = \frac{|E_{i,\text{left}} + E_{\text{iso}}| + |E_{i,\text{right}} - E_{\text{iso}}|}{2}. \tag{82}$$

The energy deviations E_1, E_2 and E_3 resulting from hyperfine splitting can now be calculated for all the fitting models. They are summarized in Table 5.

Tab. 5: In the table, for the three fitting functions being sums of Gaussian, Lorentz or Voigt profiles, the energy deviations E_1, E_2 and E_3 resulting from hyperfine splitting are summerized.

Model	E_1 [neV]	E_2 [neV]	E_3 [neV]
Gauß	35 ± 7	152 ± 4	258 ± 4
Lorentz	36 ± 7	150 ± 4	258 ± 4
Voigt	35 ± 7	151 ± 4	258 ± 4

All three models are very good compatible with each other, for the third energy we even find the same value for all three models. This shows, that although there are quite high uncertainties on the measured data points, the positions of the peaks seem to be determined properly. This can be used to get an accurate value for the magnetic field and moment in the following section.

4.6.2 Magnetic field and magnetic moment

As derived in the theory part, the three energy shifts observed in the hyperfine splitting can be directly connected to the magnetic moment μ_g and μ_e of the ground and excited state, as well as the magnetic field B:

$$E_3 = (\mu_g - \mu_e) \cdot B, \tag{83}$$

$$E_2 = (\mu_g - \frac{1}{3}\mu_e) \cdot B, \tag{84}$$

$$E_1 = (\mu_g + \frac{1}{3}\mu_e) \cdot B. \tag{85}$$

From these equations, one can directly find an expression for the magnetic field by adding the last two equations:

$$B = \frac{E_1 + E_2}{2\mu_g}. \tag{86}$$

We therefore only need a value for the magnetic moment of the ground state. Using $\mu_g = 0.090\,44 \pm 0.000\,07\mu_N$ [21] with the nuclear magneton $\mu_N = 3.152\,45 \times 10^{-8}\,\mathrm{eV\,T^{-1}}$ [13], we get the following results for the magnetic field using Gaussian error propagation for the uncertainty:

$$B_G = (32.7 \pm 1.4)\,\mathrm{T}, \tag{87}$$

$$B_L = (32.6 \pm 1.4)\,\mathrm{T}, \tag{88}$$

$$B_V = (32.7 \pm 1.4)\,\mathrm{T}. \tag{89}$$

We can perform a comparison with a literature value for the magnetic field taken from [20]:

$$B_{\mathrm{lit}} = 33.0\,\mathrm{T}. \tag{90}$$

All three values are very good compatible with the literature value with t-values all being smaller than 0.3. In addition, all relative uncertainties are smaller than 5 %. This again supports, that the peak positions could be found very precisely even though high uncertainties on the rates complicate the fitting. For the magnetic moment, the remaining formula can be used:

$$\mu_e = \mu_g - \frac{E_3}{B}. \tag{91}$$

Inserting the values and performing Gaussian error propagation we find, in units of the nuclear magneton μ_N:

$$\mu_{e,G} = (-0.160 \pm 0.012)\,\mu_N, \tag{92}$$

$$\mu_{e,L} = (-0.160 \pm 0.012)\,\mu_N, \tag{93}$$

$$\mu_{e,V} = (-0.160 \pm 0.011)\,\mu_N. \tag{94}$$

A comparison with the literature value [21]

$$\mu_{e,\mathrm{lit}} = (-0.1549 \pm 0.0002)\,\mu_N, \tag{95}$$

again shows a good compatibility for all three models with t-values of less than 0.5.

4.6.3 Effective thickness

For further evaluations, the effective absorber thickness is needed again. Using Equation 59, it can be directly calculated from values presented in literature. In comparison to the stainless steel

absorber, the only value that change is the fraction of iron in the material, with $p = (98 \pm 2)\,\%$ [17][2] for the natural iron absorber. In analogy to the calculation for stainless steel we now find:

$$T_A = 9.0 \pm 0.3. \tag{96}$$

As explained in the theory part, for a split absorption spectrum, the effective absorber thickness needs to be weighted with the corresponding peak intensity. We therefore find different effective absorber thicknesses for the different peaks of the spectrum. With intensities $I = \dot{N}(\infty) - \dot{N}(\mu)$ and normalization $N = \sum_j I_j$ we find the following absorber thicknesses:

$$T_{A,j} = W_j T_A \quad \text{with} \quad W_j = \frac{I_j}{N}. \tag{97}$$

All weights W_j and absorber thicknesses $T_{A,j}$ are summerized in Table 6, as presented on the following page.

4.6.4 Debye-Waller factor

To determine the Debye-Waller factor, we use the same procedure as presented for the stainless steel absorber. Again, for every peak, first the difference between minimal and maximal rate, as well as the y-intercept are found using the fit parameters. Together with the effective absorber thickness from the previous section, which is individual for every peak due to the weights, the values are inserted into Equation 65 to determine the Debye-Waller factor and into Equation 66 to calculate the uncertainty. The values for all the peaks and all three fitting models are summarized in Table 6, where also the weights and effective absorber thicknesses are presented.

[2]The data could not be found in another source and is therefore taken from the instructions.

Tab. 6: The table contains the weights of the peaks in the natural iron spectrum calculated from the intensity and the corresponding effective absorber thicknesses and Debye-Waller factors. The values are computed with the parameters of different fitting functions – a sum of six Gauß, Lorentz and Voigt functions.

j	W_j	$T_{A,j}$	$f_{A,j}$
Gauß			
Peak 1, right	0.16 ± 0.10	1.5 ± 0.3	0.08 ± 0.02
Peak 1, left	0.11 ± 0.06	1.0 ± 0.3	0.08 ± 0.03
Peak 2, right	0.10 ± 0.07	0.9 ± 0.3	0.09 ± 0.05
Peak 2, left	0.18 ± 0.06	1.6 ± 0.3	0.05 ± 0.02
Peak 3, right	0.27 ± 0.09	2.4 ± 0.3	0.165 ± 0.018
Peak 3, left	0.18 ± 0.08	1.6 ± 0.3	0.16 ± 0.03
Lorentz			
Peak 1, right	0.19 ± 0.15	1.7 ± 0.3	0.11 ± 0.03
Peak 1, left	0.09 ± 0.06	0.8 ± 0.3	0.10 ± 0.06
Peak 2, right	0.09 ± 0.08	0.8 ± 0.3	0.11 ± 0.07
Peak 2, left	0.15 ± 0.07	1.4 ± 0.3	0.07 ± 0.03
Peak 3, right	0.27 ± 0.13	2.4 ± 0.3	0.20 ± 0.03
Peak 3, left	0.20 ± 0.12	1.8 ± 0.3	0.19 ± 0.03
Voigt			
Peak 1, right	0.1 ± 0.4	1.3 ± 0.4	0.09 ± 0.05
Peak 1, left	0.12 ± 0.13	1.1 ± 0.3	0.08 ± 0.04
Peak 2, right	0.09 ± 0.17	0.8 ± 0.3	0.10 ± 0.08
Peak 2, left	0.19 ± 0.15	1.7 ± 0.3	0.05 ± 0.04
Peak 3, right	0.3 ± 0.3	2.7 ± 0.4	0.18 ± 0.04
Peak 3, left	0.2 ± 0.2	1.4 ± 0.3	0.17 ± 0.05

It is important to notice, that for all three models very similar results are found, with nearly all values being compatible between the different models in the range of the uncertainties. This may be due to the fact, that in general, the fits of all three models to the spectrum result in very similar peak shapes, as can be seen in Figure 14. Therefore, also all the information taken from the peak shape will be quite similar.

For the Debye-Waller factor, again no literature values can be found. However, with maximal factors of 20 % and several lower values, the fraction of recoilless absorptions seems to be a bit lower than for the stainless steel absorber. However, also the relative uncertainties are significantly higher than for stainless steel. This may be due to the fact, that also the uncertainties on the normalisation now is a lot higher than for the stainless steel absorber. For the Debye-Waller factor, we have a lot of values, having an error in the order of magnitude of the value itself. Due to quite low counting rates, most of the peaks are only vaguely visible. The data would be also compatible with a flat profile without a peak within the uncertainty. It will be part of the discussing if this might be a source for the high relative uncertainties.

4.6.5 Linewidth and lifetime

In a last step, again the lifetimes of the states are examined, using a similar procedure as for stainless steel. First, the FWHM value for the corresponding model is calculated and afterwards

corrected, using the effective absorber thickness for every peak and inserting it into Equation 7. From this property, finally the lifetime τ can be computed. In Table 7, all FWHM values and lifetimes are summarized, as well as t-values for the comparison with the literature value $\tau_{\text{lit}} = 141\,\text{ns}$ [20]. For the Voigt model, again two different approaches are presented. The FWHM is once calculated only using the Γ value for the FWHM from the Lorentz profile and once using the approximation formula for a Voigt profile. However, for some of the values, the profile is more or less purely Gaussian and therefore does not return useful values for the lifetime, when using the Lorentz line width. Those values are not added in the table.

Tab. 7: The table contains the FWHM of the fitted Gauß, Lorentz and Voigt functions and the corresponding lifetime. Moreover, the corrected natural linewidth, the corresponding lifetime and the t-values are calculated.

Function	FWHM Γ [neV]	Lifetime τ [ns]	corr. FWHM Γ_0 [neV]	corr. Lifetime τ_0 [ns]	t-value
Gauß					
Peak 1, right	60 ± 30	12 ± 7	13 ± 8	50 ± 30	2.9
Peak 1, left	23 ± 12	28 ± 15	5 ± 3	120 ± 60	0.3
Peak 2, right	30 ± 20	21 ± 14	7 ± 5	90 ± 60	0.8
Peak 2, left	25 ± 8	26 ± 9	6 ± 2	110 ± 40	0.8
Peak 3, right	45 ± 14	14 ± 4	11 ± 3	60 ± 20	4.2
Peak 3, left	37 ± 15	18 ± 7	9 ± 4	70 ± 30	2.2
Lorentz					
Peak 1, right	60 ± 50	11 ± 9	14 ± 12	50 ± 40	2.5
Peak 1, left	20 ± 15	30 ± 20	5 ± 4	140 ± 100	0.04
Peak 2, right	30 ± 30	20 ± 20	7 ± 7	90 ± 90	0.5
Peak 2, left	20 ± 9	33 ± 15	5 ± 2	140 ± 60	0.6
Peak 3, right	40 ± 20	15 ± 6	10 ± 4	60 ± 30	2.9
Peak 3, left	40 ± 20	16 ± 9	10 ± 5	70 ± 40	1.9
Voigt, Lorentz FWHM					
Peak 1, right	0 ± 300	-	-	-	-
Peak 1, left	20 ± 20	40 ± 40	4 ± 5	150 ± 170	0.06
Peak 2, right	0 ± 130	-	-	-	-
Peak 2, left	18 ± 13	40 ± 30	4 ± 3	150 ± 110	0.12
Peak 3, right	30 ± 70	20 ± 50	7 ± 16	100 ± 200	0.2
Peak 3, left	0 ± 100	-	-	-	-
Voigt, Voigt FWHM					
Peak 1, right	50 ± 90	10 ± 20	10 ± 20	50 ± 80	1.1
Peak 1, left	20 ± 40	40 ± 70	4 ± 8	200 ± 300	0.04
Peak 2, right	30 ± 70	20 ± 50	7 ± 16	90 ± 190	0.3
Peak 2, left	20 ± 30	40 ± 60	4 ± 8	200 ± 300	0.05
Peak 3, right	40 ± 60	20 ± 20	9 ± 15	70 ± 100	0.7
Peak 3, left	40 ± 60	20 ± 30	9 ± 14	70 ± 110	0.6

First of all, we can see, that for most of the values after the correction, a value compatible with the literature value can be found. However, this is mainly due to very high relative errors, even for the Lorentz and Gauß model, where previously lower uncertainties were found for the stainless steel absorber. Again, this is mainly explained by the fact, that the fit to the data does on the one hand describe the peak position quite well, but on the other hand does not lead to a good description of the form of the peak. This is seen in the calculation of the Debye-Waller factor too and will be a main discussion point in the last part of the report.

For the Voigt fit, we again find even higher uncertainties, mainly due to the fact, that again, both – the Gauß and the Lorentz model – describe the data similarly good and a useful value

with small uncertainty can therefore not be found for σ or γ. On the benefit of the Voigt profile as a fitting function, additional considerations are added in the discussion part.

5 Discussion

5.1 Summary of Results

In the experiment, Mößbauer spectroscopy to investigate stainless steel and natural iron is performed. For this purpose, first, the used setup is optimized and calibrated. Moreover, the Compton background and the attenuation by the acrylic glass could be measured and it was possible to correct the measured data. The sledge velocity was investigated and additional systematic errors by this velocity were excluded.

The absorption spectrum of stainless steel was measured. By fitting a Gauß, a Lorentz and a Voigt function to the absorption peak, the isomeric shift E_{iso} was determined to be:

$$E_{\text{iso},G} = (10.2 \pm 1.4)\,\text{neV}, \tag{98}$$
$$E_{\text{iso},L} = (10.1 \pm 1.3)\,\text{neV}, \tag{99}$$
$$E_{\text{iso},V} = (10.2 \pm 1.3)\,\text{neV}. \tag{100}$$

Moreover, the effective absorber thickness T_A and the Debye-Waller factor f_Q of the stainless steel sample were calculated:

$$T_A = 6.4 \pm 0.5, \tag{101}$$
$$f_{Q,G} = 0.354 \pm 0.015, \tag{102}$$
$$f_{Q,L} = 0.381 \pm 0.015, \tag{103}$$
$$f_{Q,V} = 0.36 \pm 0.02. \tag{104}$$

At last, the lifetime of stainless steel was investigated:

$$\tau_G = (104 \pm 15)\,\text{ns}, \tag{105}$$
$$\tau_L = (110 \pm 20)\,\text{ns}, \tag{106}$$
$$\tau_{V,\,\text{Lorentz FWHM}} = (300 \pm 600)\,\text{ns}, \tag{107}$$
$$\tau_{V,\,\text{Voigt FWHM}} = (110 \pm 170)\,\text{ns}. \tag{108}$$

A comparison to the literature value for the lifetime shows that the value calculated with the Lorentz fit is compatible with a t-value of 1.2, while the Gauß fit provides a slightly incompatible lifetime with a t-value of 2.4. The lifetimes estimated with the Voigt fit are both compatible with a t-value of 0.3 and 0.19, but it needs to be mentioned, that it has relative errors of over 100 %.

The spectroscopy of natural iron also provides values its isomeric shift, obtained from the three different fits as before:

$$E_{\text{iso},G} = (4.3 \pm 1.4)\,\text{neV}, \tag{109}$$
$$E_{\text{iso},L} = (4.5 \pm 1.1)\,\text{neV}, \tag{110}$$
$$E_{\text{iso},V} = (4.9 \pm 1.3)\,\text{neV}. \tag{111}$$

Moreover, it was possible to determine the magnetic moment μ_e of the $I = 3/2$ state of ^{57}Fe and the internal magnetic field B:

$$\mu_{e,G} = (-0.160 \pm 0.012)\,\mu_N, \qquad B_G = (32.7 \pm 1.4)\,\text{T}, \tag{112}$$
$$\mu_{e,L} = (-0.160 \pm 0.012)\,\mu_N, \qquad B_L = (32.6 \pm 1.4)\,\text{T}, \tag{113}$$
$$\mu_{e,V} = (-0.160 \pm 0.011)\,\mu_N, \qquad B_V = (32.7 \pm 1.4)\,\text{T}. \tag{114}$$

For both properties, a comparison to literature shows very accurate results, with t-values all being smaller than 0.5. For the effective absorber thickness of the natural iron absorber

$$T_A = 9.0 \pm 0.3 \tag{115}$$

is found, which needs to be weighted with the corresponding intensity of the peak. Therefore, for every peak and every model, different values for the effective absorber thickness are found, as well as for the Debye-Waller factor, where values ranging from 5 % to 20 % are calculated. Those values are all smaller than for the stainless steel absorber and cannot be compared to literature.

In a last step, lifetimes are determined for all models and all peaks, which are summerized in Table 7. They are all compatible with literature, but show significantly larger relative errors often exceeding 100 %.

5.2 Discussion of results and uncertainties

During the experiment, the most striking problem was the low counting rate of the ^{57}Co source. In the relevant energy window, the source only provided a counting rate of approximately 1 Bq when background corrected. As the relative statistical uncertainty of the rate is $\sqrt{N}/t$, it is necessary to measure a lot of counts to reduce those uncertainties. Because of the low counting rate, this needs a very long measurement time for every sledge velocity. In the limited time range given for this experiment, the relative statistical uncertainties could only be reduced to approximately 5 %. The main reason for the low counting rate might be the age of the source, which is older than several lifetimes of the emitter. The half-life of the source is only approximately 200 days.

Moreover, it was difficult to generate more measurement time with overnight measurements, as the measurement device with the sledge crashed after sometime due to unknown error. It looks like there is a problem with the LabView program or the sledge motor. The interruptions appeared unpredictably, making it difficult to plan measurements over long times. Together with the low counting rates, this problem hindered to achieve a sufficiently small statistical uncertainties.

Resulting from the low counting rate, the spectrum measured for the adjustment of the energy window was quite low in intensity especially, since the maximal number of channels was used to measure the whole spectral range. Thus, the counts per channel were particularly small. The height of the peak was comparable with the background intensity. This can cause errors in the fit of the peak position, which might result in an incorrect adjusted energy window. However, the fitted peak position was still compatible with the literature value, showing that the energy window seemed to be set correctly. It was adjusted with a width of 2σ of the fit. This approach seems to be reasonable, as in this area there should be 95 % of the events. Outside of this range there was a next peak visible when observing the spectrum in the software, which was excluded by the 2σ range. A wider energy window would have lead to a higher counting rate, but then there could also be photons included, which belong to another transition or would mainly include background.

For the Mößbauer spectroscopy itself, the comparatively low counting rates for each velocity lead to a quite noisy spectrum. Therefore, some peaks were not clearly identifiable and the uncertainties – especially for the natural iron sample – were in a similar order of magnitude as the peak minima. As a result, the fitting uncertainties on the peak intensity, the y-intercept and the width parameters were quite high. This is reasonable, when looking at the measured spectra: The uncertainties on the values are high enough, that a change in one of the parameters would

lead to a fit, still being compatible within the uncertainties. This also affects all quantities resulting from the width parameter, the intensity or the y-intercept, which are mainly the lifetime and the effective absorber thickness. For stainless steel, where the uncertainties are smaller compared to the peak minimum, this results in values still compatible with literature but with rather high relative uncertainties. For the natural iron absorber, however, the lifetime deviates a lot from literature and is only compatible because of the huge relative uncertainties.

Nevertheless, the fits provide quite good estimates for the peak positions. The resulting quantities as the magnetic moment and the internal magnetic field can therefore be determined with small relative errors and are within their uncertainties compatible with literature values.

When fitting the Voigt function, it is also striking that the lifetime calculated with the fit parameter γ, which gives the width of the Lorentz function and therefore should account for the natural linewidth, has high uncertainties and also provides unreasonable results. This might be due to the fact that the data does not allow a distinction of the peak shape in Gaussian or Lorentzian. The high uncertainty and the high anti-correlation of γ and σ confirm this, as changing both parameters in a way, that the width stays constant would also lead to reasonable fits. This could be included in the uncertainty by adding a correlation term in the error calculations. Nevertheless, the value of γ obtained by the fit does not provide information about the physical linewidth and is therefore not useful for further calculations. The FWHM of the Voigt fit, which is taken as linewidth does, as the Gauß and the Lorentz fit, not contain information about the natural linewidth. Therefore, this model only adds parameters to the fit but does not provide further information. For this reason, it is not reasonable to use a Voigt function as fit to the data measured in this experiment.

Additionally to the already mentioned statistical uncertainties, there are also systematic uncertainties from background subtraction and the attenuation of acrylic glass. However, these uncertainties only play a minor role as they are approximately 2 % of the value and therefore smaller than the statistical errors. Besides these two systematic error sources, there could also be a systematic error resulting from the sledge velocity. We performed several measurements and within the achieved uncertainties, these measurements are compatible with the assumption of the velocity being set correctly by the software. There might be more systematic errors in the measurement, but because of the dominating statistical uncertainties it is hard to identify them.

References

[1] Fritz Parak: *Rudolf L. Mößbauer* in *Nature, Vol. 478*, (2011)

[2] Goester Klingelhoefer et. al.: *Moessbauer Spectroscopy of Soils and Rocks at Gusev Crater and Meridiani Planum* (2004)

[3] Paul A. Tipler, Gene Mosca: *Physik, Kapitel 12.4 – Der Doppler-Effekt*, (Berlin, Heidelberg, 2015)

[4] Bogdan Povh et al.: *Teilchen und Kerne – Eine Einführung in die physikalischen Konzepte*, 9. edition, Springer, (Berlin, Heidelberg: 2013)

[5] Caltech: *The Mossbauer effect: hyperfine splitting*, (accessed: 25.04.2024)

[6] P. Busch: *The Time-Energy Uncertainty Relation* in *Time in Quantum Mechanics. Lecture Notes in Physics, vol 72. Springer*, (Berlin, Heidelberg: 2002)

[7] J. Hebler: *Linewidth of Mößbauer Absorption* in *Nuclear Instruments and Methods in Physics Reserach, Vol 58*, (Amsterdam, London: 1967)

[8] S. Margulies, P. Debrunner, H. Frauenfelder: *Transmission and Line Broadening in the Mößbauer Effect. II* in *Nuclear Instruments and Methods in Physics Reserach, Vol 21*, (Amsterdam, London: 1962)

[9] O, C. Kistner, A. W. Sunyar: *Evidence for Quadrupole Interaction of* Fe^{57m} *and influence of chemical binding on nuclear gamma-ray energy*, (New York, 1960)

[10] Shirley, D. A.: *Application and interpretation of isomer shifts* in *Reviews of Modern Physics, Vol. 36*, (1964)

[11] Caltech: *The Mossbauer effect: Hyperfine splitting*, http://www.sophphx.caltech.edu/Physics_7/Experiment_29.pdf, (accessed: 22.04.2024)

[12] Wolfgang Demtröder: *Experimentalphysik 4 - Kern-, Teilchen- und Astrophysik*, edition 5, (Berlin, Heidelberg: 2017)

[13] W. M. Haynes: *CRC handbook of chemistry and physics, 95th edition*, (Boca Raton: 2014-15)

[14] James E. Parks: *Attenuation of Radiation*, (Tennessee, 2001)

[15] Charles Kittel: *Introduction to Solid State Physics*, edition 8, (Hoboken: 2005)

[16] Virtanen, Pauli et. al.; SciPy 1.0 Contributors: *SciPy 1.0: Fundamental Algorithms for Scientific Computing in Python* in *Nature Methods*, (2020)

[17] A. Zwerger, S. Winkelmann, M. Köhli, J. Wollrath: *Mößbauer-Effect – Versuchsanleitung Fortgeschrittenen Praktikum Teil 2*, (Freiburg im Breisgau: 2017)

[18] V. P. Chechev, N. K. Kuzmenko: *Table de radionucleides* ${}^{57}_{27}Co_30$, (2001)

[19] J. J. Olivero, R. L. Longbothum: *Empirical fits to the Voigt line width: A brief review* in *Journal of Quantitative Spectroscopy and Radiative Transfer* (The Pennsylvania State University: 1977)

[20] Brent Fultz: *Mössbauer Spectrometry*, California Institute of Technology, (Pasadena: 2011)

[21] Pramila Raghavan: *Table of Nuclear Moments*, Academic press Inc., (1989)

7 Appendix

7.1 Tables and graphics

7.1.1 Table with the used symbols in the protocol

Tab. 8: Table of the used symbols for the parameters used in the protocol. The constants are all taken from [13].

Symbol	Parameter
f_a, f_e	absorber/emitter frequency (Doppler effect)
m	mass
v	velocity
R	recoil
c	channel number
N	number of counts
$\dot{N}, \dot{N}_C$	rate, Compton rate
T	transmission
μ/ρ	absorption coefficient
d	absorber thickness
E_{iso}	isomeric shift
$E_{1,2,3}$	energy shifts resulting from hyperfine splittig
B, μ	magnetic field, magnetic moment
m_I, I	magnetic quantum numbers
$f_{A/Q}$	Debye-Waller factor of absorber/source
I_i, W_i	intensity and relative intensity of peak i
$T_{A/Q}$	effective absorber/source thickness
n	number density
ρ	density
M	molar mass
p	iron content in the absorber
β	fraction of isotope in the element
σ	cross section
α	conversion coefficient of a transition
Γ	full width half maximum (FWHM)
τ	lifetime
A, y_0	fitting parameter: amplitude and y-intercept
μ	fitting parameter: mean
σ, γ	fitting parameter: width
a, b	fitting parameters in linear models
t, χ^2	t-value, (reduced) χ^2-value
Constants	
$c = 2.997\,925 \times 10^{8}\,\mathrm{m\,s^{-1}}$	speed of light
$h = 6.626\,070 \times 10^{-34}\,\mathrm{J\,s}$	Planck constant
$N_A = 6.022\,141 \times 10^{23}\,\mathrm{mol^{-1}}$	Avogadro constant
$\mu_N = 3.152\,45 \times 10^{-8}\,\mathrm{eV\,T^{-1}}$	nuclear magneton

7.1.2 Graphics

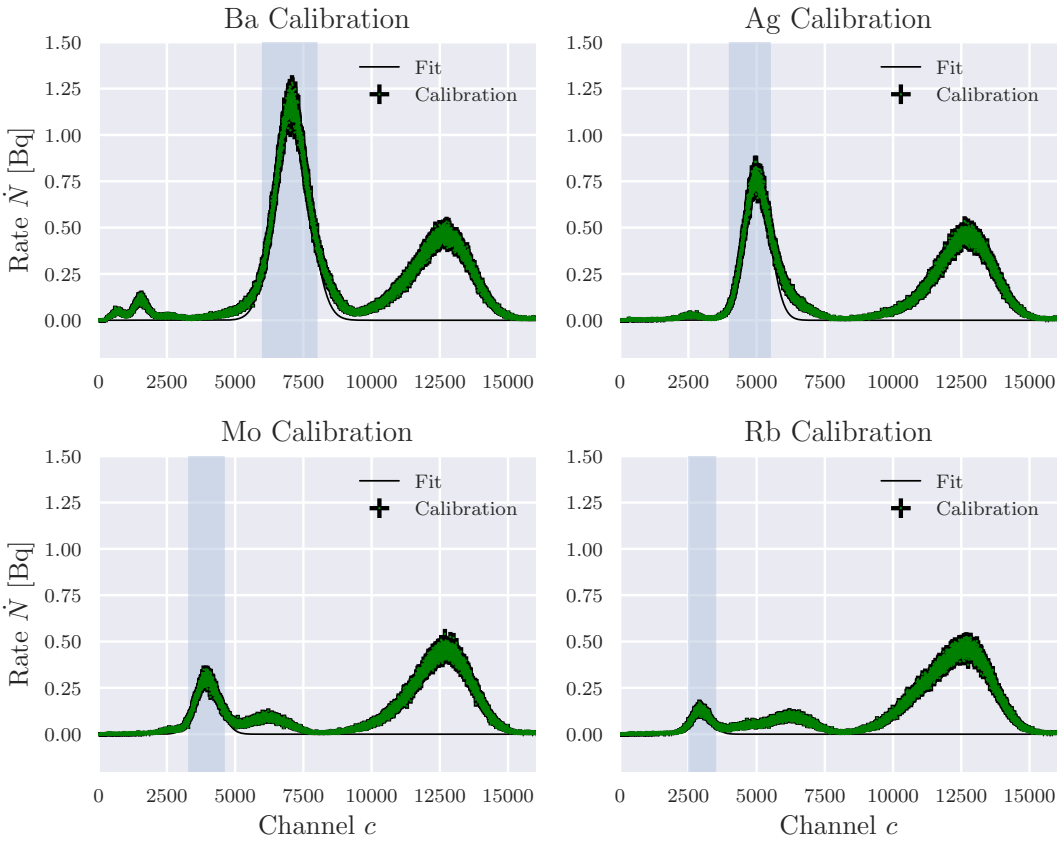

Fig. 15: In the graphic, the measured spectra with the MCA of the additional calibration absorbers are presented. One can find the spectra of Ba, Ag, Mo and Rb in the graphics. For all plots, the rate $\dot{N}$ in $\mathrm{Bq} = \mathrm{s}^{-1}$ is plotted against the arbitrary channel number c. The green data points are presented with black error bars. In addition, the fitted Gaussian is presented, with the fitting area marked in grey.

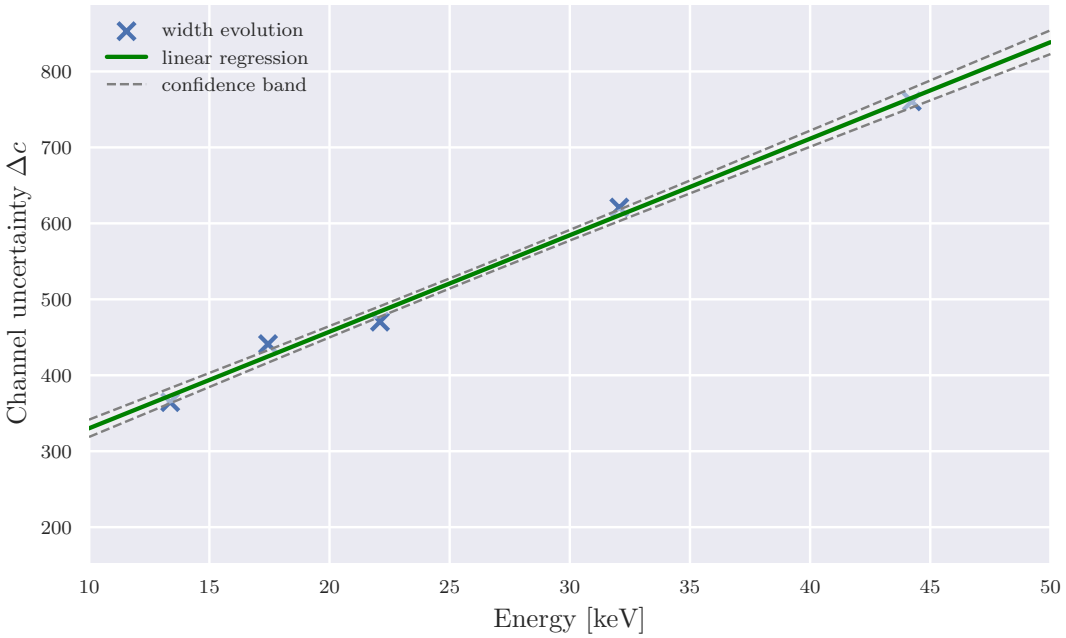

Fig. 16: In the plot, the linear regression used to estimate the width of the 14.4 keV peak can be found, with the measured channel uncertainty Δc plotted against the known energy E in keV. The channel uncertainty is equivalent to the fitting parameter σ. In addition to the data, the linear regression is portrayed with a corresponding confidence band. The uncertainties are not plotted and used for the fit, since the main use of this regression is to get a rough estimate for the channel width of the desired peak.

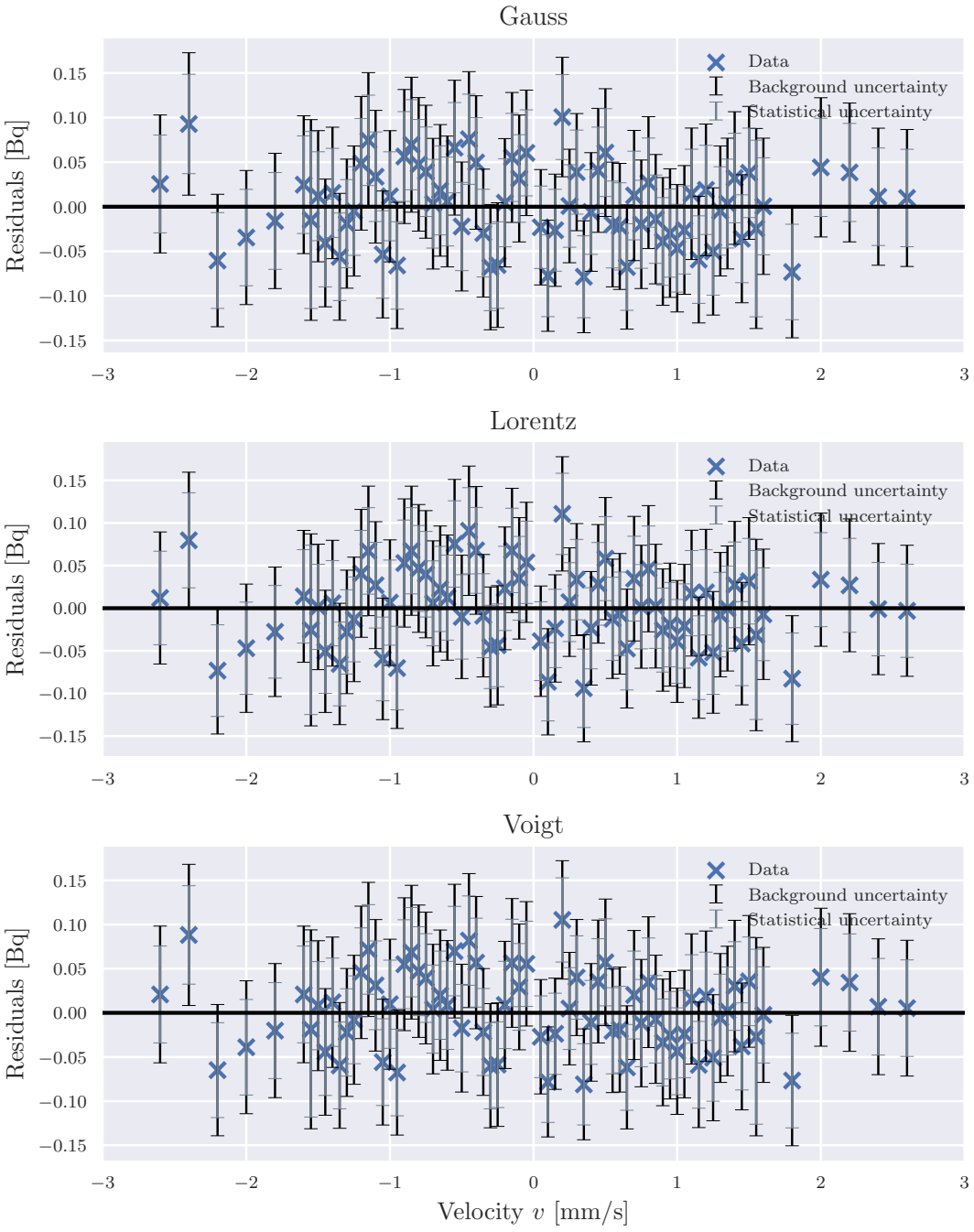

Fig. 17: In the three graphics, the residuals of the fits for the three models of a Gaussian, Lorentz and Voigt fit are shown for the stainless steel absorber. The residuals in $\mathrm{Bq} = \mathrm{s}^{-1}$ are plotted against the velocity v in $\mathrm{mm\,s}^{-1}$. The uncertainties are split into statistical and systematical background uncertainties. Most of the values are compatible with the zero, leading to a low χ^2 value for the fit.

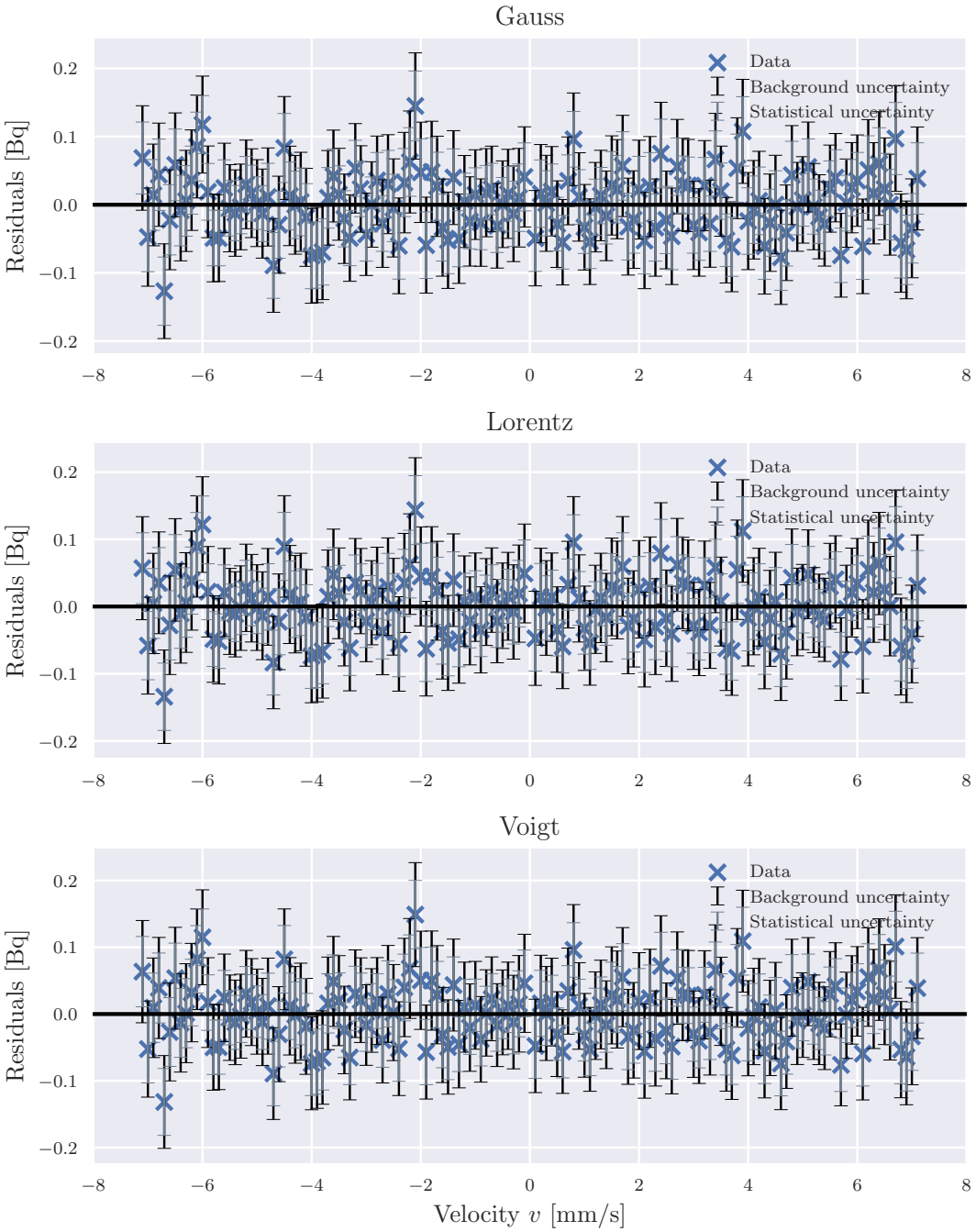

Fig. 18: In the three graphics, the residuals of the fits for the three models of a sum of six Gaussian, Lorentz and Voigt profiles are shown for the natural iron absorber. The residuals in Bq = s^{-1} are plotted against the velocity v in $mm\,s^{-1}$. The uncertainties are split into statistical and systematical background uncertainties. Most of the values are compatible with the zero, leading to a low χ^2 value for the fit.

7.1.3 Tables

Tab. 9: The table contains the fitting parameters of the sum of 6 Gaussian functions to the natural iron spectrum. The peaks are numbered starting from the interior peaks. The y-intercept is fitted as $y_0 = (0.994 \pm 0.011)\,\mathrm{Bq}$ and the reduced χ^2 values is $\chi^2_{red} = 0.48$.

Gauß	μ in $\mathrm{mm\,s^{-1}}$	σ in $\mathrm{mm\,s^{-1}}$	A in Bq
Peak 1, right	0.8 ± 0.3	0.5 ± 0.3	0.08 ± 0.05
Peak 1, left	-0.64 ± 0.10	0.20 ± 0.11	0.05 ± 0.02
Peak 2, right	3.31 ± 0.17	0.27 ± 0.18	0.05 ± 0.03
Peak 2, left	-3.00 ± 0.07	0.22 ± 0.07	0.08 ± 0.03
Peak 3, right	5.40 ± 0.11	0.40 ± 0.12	0.13 ± 0.04
Peak 3, left	-5.33 ± 0.12	0.33 ± 0.13	0.08 ± 0.03

Tab. 10: The table contains the fitting parameters of the sum of 6 Lorentz functions to the natural iron spectrum. The peaks are numbered starting from the interior peaks. The y-intercept is fitted as $y_0 = (1.01 \pm 0.02)\,\mathrm{Bq}$ and the reduced χ^2 values is $\chi^2_{red} = 0.48$.

Lorentz	μ in $\mathrm{mm\,s^{-1}}$	γ in $\mathrm{mm\,s^{-1}}$	A in Bq
Peak 1, right	0.9 ± 0.3	0.6 ± 0.5	0.15 ± 0.12
Peak 1, left	-0.63 ± 0.10	0.21 ± 0.16	0.07 ± 0.05
Peak 2, right	3.26 ± 0.17	0.3 ± 0.3	0.07 ± 0.06
Peak 2, left	-3.00 ± 0.06	0.21 ± 0.09	0.12 ± 0.05
Peak 3, right	5.41 ± 0.11	0.5 ± 0.2	0.21 ± 0.09
Peak 3, left	-5.34 ± 0.13	0.4 ± 0.2	0.19 ± 0.08

Tab. 11: The table contains the fitting parameters of the sum of 6 Voigt functions to the natural iron spectrum. The peaks are numbered starting from the interior peaks. The y-intercept is fitted as $y_0 = (1.00 \pm 0.03)\,\mathrm{Bq}$ and the reduced χ^2 values is $\chi^2_{red} = 0.50$.

Voigt	μ in $\mathrm{mm\,s^{-1}}$	σ in $\mathrm{mm\,s^{-1}}$	γ in $\mathrm{mm\,s^{-1}}$	A in Bq
Peak 1, right	0.8 ± 0.3	0.5 ± 1.4	0 ± 3	0.08 ± 0.19
Peak 1, left	-0.62 ± 0.09	$(0 \pm 2) \times 10^6$	0.2 ± 0.2	0.07 ± 0.06
Peak 2, right	3.30 ± 0.17	0.3 ± 0.7	0.0 ± 1.3	0.05 ± 0.09
Peak 2, left	-3.00 ± 0.05	$(0 \pm 2) \times 10^6$	0.18 ± 0.13	0.11 ± 0.05
Peak 3, right	5.41 ± 0.11	0.2 ± 0.6	0.3 ± 0.7	0.17 ± 0.14
Peak 3, left	-5.33 ± 0.12	0.3 ± 0.5	0.0 ± 1.0	0.09 ± 0.12

7.2 Code

[ ]:
```
# Importing necessary libraries

import matplotlib.pyplot as plt
import numpy as np
from scipy.optimize import curve_fit
from scipy.special import voigt_profile
```

[ ]:
```
# Adapt style of the plots
plt.style.use('seaborn-v0_8')

tex_fonts = {
    "text.usetex": True,
    "font.family": "serif",
    "axes.labelsize": 11,
    "font.size": 11,
    "legend.fontsize": 8,
    "xtick.labelsize": 8,
    "ytick.labelsize": 8
}

plt.rcParams.update(tex_fonts)

def set_size(width='page', fraction=1, subplots=(1, 1), ratio=(5**.5 - 1) /␣
 ↪2):
    if width == 'page':
        width_pt = 455.0
    elif width == 'col':
        width_pt = 246.0
    else:
        width_pt = width

    fig_width_pt = width_pt * fraction
    inches_per_pt = 1 / 72.27

    fig_width_in = fig_width_pt * inches_per_pt
    fig_height_in = fig_width_in * ratio * (subplots[0] / subplots[1])

    return (fig_width_in, fig_height_in)
```

[ ]:
```
# Definitions of useful functions

# Gaussian profile for fit
def gauss(x, A, mu, sig_squared):
    return A*np.exp(-(x-mu)**2/(2*sig_squared))

# Calculation of chi^2
def chiq(y, y_err, mod_y):
    return sum([(j-i)**2/delj**2 for i,j,delj in zip(y, mod_y, y_err)])
```

```
# Calculation of reduced chi^2
def red_chiq(y, y_err, mod_y, par):
    return chiq(y, y_err, mod_y)/(len(y)-par)

# Functions to plot linear models with confidence band
def Modell(xbereich, p):
    return [p[0]*i+p[1] for i in xbereich]

def Konfidenz(xbereich, p, Vp):
    des = [np.sqrt(np.matmul(np.transpose(np.array([i, 1])),np.matmul(Vp,np.
 ↪array([i, 1])))) for i in xbereich]
    return [[p[0]*i+p[1]+des[j] for i,j in␣
 ↪zip(xbereich,range(len(xbereich)))],[p[0]*i+p[1]-des[j] for i,j in␣
 ↪zip(xbereich,range(len(xbereich)))]]
```

7.2.1 Calibration

[ ]:
```
# Function reading in data
def read(file):
    with open(file, "r") as doc:
        string = doc.read()
        Zeilen = string.split("\n")
        Zeilen.pop(0)
        Zeilen.pop(0)
        Zeilen.pop(-1)
        counts = []
        for z in Zeilen:
            eintrag = z.split(",")
            counts.append(int(eintrag[0]))
        channel = list(range(len(counts)))
    return [channel, counts]
```

[ ]:
```
# Reading in Calibration data and defining calibration points

cal_tb = read("calibration_Tb_2.TKA")
cal_rb = read("calibration_Rb_2.TKA")
cal_mo = read("calibration_Mo_2.TKA")
cal_ba = read("calibration_Ba_2.TKA")
cal_ag = read("calibration_Ag_2.TKA")

t_cal = 750

cal_channel = [0, 0, 0, 0, 0]
cal_sig = [0, 0, 0, 0, 0]
cal_energy = [13.37, 17.44, 22.10, 32.06, 44.23]
```

Spectra of calibration sources

[ ]:
```
# Plot of Tb Calibration

x0 = np.array(cal_tb[0])
```

```
y0 = np.array(cal_tb[1])/t_cal
y0_err = np.sqrt(np.array(cal_tb[1]))/t_cal

window0 = [8500, 10500]

fig, ax = plt.subplots(1, 1, figsize=set_size())

ax.errorbar(x0, y0, xerr=1/np.sqrt(3), yerr=y0_err, ecolor="black",␣
↪marker="o", ls="", markersize=1, label="Tb Calibration", color="green")
ax.fill_betweenx([-0.5,3.5], window0[0], window0[1], color="lightsteelblue",␣
↪alpha=0.5)

popt0, pcov0 = curve_fit(gauss, x0[window0[0]: window0[1]], y0[window0[0]:␣
↪window0[1]], sigma=y0_err[window0[0]: window0[1]], p0=[1, 10000, 500],␣
↪absolute_sigma=True)
ax.plot(np.linspace(0,16000,1000), gauss(np.linspace(0,16000,1000),␣
↪popt0[0], popt0[1], popt0[2]), color="black", label="Fit")

cal_channel[4] = popt0[1]
cal_sig[4] = np.sqrt(popt0[2])

ax.legend()
ax.grid()
ax.set_ylim(-0.2, 2.0)
ax.set_xlim(0, 16000)
ax.grid()
ax.set(xlabel="Channel $c$", ylabel="Rate $\dot{N}$ [Bq]")

plt.savefig("4_2_cal_Tb.pdf", format="pdf", bbox_inches='tight')
plt.show()
```

[ ]:
```
# Plot of other Calibrations

x = np.array([cal_ba[0], cal_ag[0], cal_mo[0], cal_rb[0]])
y = np.array([cal_ba[1], cal_ag[1], cal_mo[1], cal_rb[1]])/t_cal
y_err = np.sqrt(np.array([cal_ba[1], cal_ag[1], cal_mo[1], cal_rb[1]]))/t_cal
window = np.array([[6000, 8000], [4000, 5500], [3300, 4600], [2500, 3500]])

guess = [7000, 5000, 4000, 2700]

popt, pcov = [], []
for i in range(4):
    p, pV = curve_fit(gauss, x[i][window[i][0]: window[i][1]],␣
↪y[i][window[i][0]: window[i][1]], sigma=y_err[i][window[i][0]:␣
↪window[i][1]], p0=[1, guess[i], 500], absolute_sigma=True)
    popt.append(p)
    pcov.append(pV)
    cal_channel[3-i] = popt[i][1]
    cal_sig[3-i] = np.sqrt(popt[i][2])
```

```
fig, axs = plt.subplots(2, 2, figsize=set_size("page", subplots=(2, 2),␣
↪ratio=0.8))

title=["Ba Calibration", "Ag Calibration", "Mo Calibration", "Rb␣
↪Calibration"]

for i, ax in enumerate(fig.get_axes()):
        ax.errorbar(x[i], y[i], xerr=1/np.sqrt(3), yerr=y_err[i],␣
↪ecolor="black", marker="o", ls="", markersize=1, label="Calibration",␣
↪color="green")
        ax.fill_betweenx([-0.5,3.5], window[i][0], window[i][1],␣
↪color="lightsteelblue", alpha=0.5)
        ax.plot(np.linspace(0,16000,1000), gauss(np.linspace(0,16000,1000),␣
↪popt[i][0], popt[i][1], popt[i][2]), color="black", linewidth=0.7,␣
↪label="Fit")
        ax.legend()
        ax.set_xlim(0,16000)
        ax.set_ylim(-0.2,1.5)
        ax.set_title(title[i])

axs[0, 0].set(ylabel="Rate $\dot{N}$ [Bq]")
axs[1, 0].set(ylabel="Rate $\dot{N}$ [Bq]", xlabel="Channel $c$")
axs[1, 1].set(xlabel="Channel $c$")

plt.tight_layout()
plt.savefig("4_2_calibration_other.pdf", format="pdf", bbox_inches='tight')
plt.show()
```

Linear regressions

[ ]:
```
# Plot of linear regression for Calibration

fig, ax = plt.subplots(1, 1, figsize=set_size())

ax.scatter(cal_channel, cal_energy, marker="x", label="calibration")
ax.errorbar(cal_channel, cal_energy, xerr=cal_sig, ecolor="black", ls="",␣
↪capsize=3)

def f(x,a,b):
        return a*x+b

p_cal, Vp_cal = curve_fit(f, cal_channel, cal_energy)
x = np.linspace(2000,12000,5000)
mod = Modell(x,p_cal)
konf = Konfidenz(x,p_cal,Vp_cal)
ax.plot(x, mod, label="linear regression", color="green")
ax.plot(x, konf[0], linestyle="dashed", linewidth=1, color="grey",␣
↪label="confidence band")
ax.plot(x, konf[1], linestyle="dashed", linewidth=1, color="grey")
ax.fill_between(x, konf[0], konf[1], color="whitesmoke", alpha=0.5)
```

```
ax.legend()
ax.set_xlim(2000, 12000)
ax.set(ylabel="Energy [keV]", xlabel="Channel $c$")

plt.tight_layout()
plt.savefig("4_2_calibration_linreg.pdf", format="pdf", bbox_inches='tight')
plt.show()

def calibration(channel, channel_err=1/np.sqrt(3)):
    E = channel*p_cal[0]+p_cal[1]
    del_E = np.sqrt(p_cal[0]**2*channel_err**2+channel**2*Vp_cal[0,␣
 ↪0]+Vp_cal[1, 1]+2*channel*Vp_cal[0][1])
    return E, del_E
```

[ ]:
```
# Plot of linear model on peak widths

fig, ax = plt.subplots(1, 1, figsize=set_size())

ax.scatter(cal_energy, cal_sig, marker="x", label="width evolution")
ax.errorbar(cal_energy, cal_sig, ecolor="black", ls="", capsize=3)

def f(x,a,b):
        return a*x+b

p_sig, Vp_sig = curve_fit(f, cal_energy, cal_sig)
x = np.linspace(0,50,5000)
mod = Modell(x,p_sig)
konf = Konfidenz(x,p_sig,Vp_sig)
ax.plot(x, mod, label="linear regression", color="green")
ax.plot(x, konf[0], linestyle="dashed", linewidth=1, color="grey",␣
 ↪label="confidence band")
ax.plot(x, konf[1], linestyle="dashed", linewidth=1, color="grey")
ax.fill_between(x, konf[0], konf[1], color="whitesmoke", alpha=0.5)

ax.legend()
ax.set_xlim(10, 50)
ax.set(xlabel="Energy [keV]", ylabel = "Channel uncertainty $\\Delta c$")

plt.tight_layout()
plt.savefig("4_2_width_evolution.pdf", format="pdf", bbox_inches='tight')
plt.show()
```

7.2.2 Spectrum of Co

with and without the energy window

[ ]:
```
# Read in data from Co spectrum

spec = read("spectrum_Co_2.TKA")
peak = read("peak_Co_error.TKA")[0], np.array(read("peak_Co_error.
 ↪TKA")[1])+np.array(read("peak_Co_2.TKA")[1])
```

```
t_spec = 3292
```

[ ]:
```
# Plots of Co spectrum

fig, axs = plt.subplots(1, 2, figsize=set_size("page", subplots=(1, 2),␣
 ↪ratio=0.8))

window = [2700,3600]
axs[0].fill_betweenx([-0.5,40], calibration(window[0])[0],␣
 ↪calibration(window[1])[0], color="lightsteelblue", alpha=0.5)

x = calibration(np.array(spec[0]))[0]
x_err = calibration(np.array(spec[0]))[1]
y = np.array(spec[1])
y_err = np.sqrt(np.array(spec[1]))

axs[0].errorbar(x, y, xerr=x_err, yerr=y_err, ecolor="black", marker="o",␣
 ↪ls="", markersize=1, label="Spectrum", color="green")

popt, pcov = curve_fit(gauss, x[window[0]: window[1]], y[window[0]:␣
 ↪window[1]], sigma=y_err[window[0]: window[1]], p0=[20, 14, 4],␣
 ↪absolute_sigma=True)
axs[0].plot(np.linspace(0,70,1000), gauss(np.linspace(0,70,1000), popt[0],␣
 ↪popt[1], popt[2]), label="Fit", color="red")
axs[0].set_ylim(0, 30)
axs[0].set(ylabel="counts $N$")

window = [2500,3900]
axs[1].fill_betweenx([-0.5,65], calibration(window[0])[0],␣
 ↪calibration(window[1])[0], color="lightsteelblue", alpha=0.5)

x = calibration(np.array(peak[0]))[0]
x_err = calibration(np.array(peak[0]))[1]
y = np.array(peak[1])
y_err = np.sqrt(np.array(peak[1]))

axs[1].errorbar(x, y, xerr=x_err, yerr=y_err, ecolor="black", marker="o",␣
 ↪ls="", markersize=1, label="Spectrum", color="green")

popt, pcov = curve_fit(gauss, x[window[0]: window[1]], y[window[0]:␣
 ↪window[1]], sigma=y_err[window[0]: window[1]], p0=[1, 15, 4],␣
 ↪absolute_sigma=True)
axs[1].plot(np.linspace(0,70,1000), gauss(np.linspace(0,70,1000), popt[0],␣
 ↪popt[1], popt[2]), label="Fit", color="red")
axs[1].set_ylim(0, 60)

for ax in fig.get_axes():
        ax.legend()
        ax.set_xlim(0,70)
```

```
        ax.set(xlabel="Energy $E$ [keV]")

plt.tight_layout()
plt.savefig("4_2_co_source.pdf", format="pdf", bbox_inches='tight')
plt.show()
```

7.2.3 Background

Compton correction

[ ]:
```
# Definition of fit function for double exponential

def double_exp(x, A, a, B, b):
    return A*np.exp(a*x)+B*np.exp(b*x)
```

[ ]:
```
# Data for Compton background measurement

counts_com = np.array([1901, 1436, 1095, 948, 792, 735, 681, 574, 641, 611,␣
↪580, 974, 541, 538, 525, 499, 517])
times_com = np.array([600.131, 604.373, 600.346, 600.342, 600.266, 600.831,␣
↪600.122, 600.455, 602.663, 600.457, 600.146, 1045.33, 599.559, 601.123,␣
↪605.357, 600.432, 600.154])
rates_com = counts_com/times_com
thickness_com = np.array([0, 0.21, 0.42, 0.63, 0.84, 1.01, 1.46, 1.96, 2.51,␣
↪3.01, 3.98, 4.99, 5.94, 6.99, 7.98, 8.99, 9.94])

rates_com_err = np.sqrt(counts_com)/times_com
thickness_com_err = 0.01
```

[ ]:
```
# Plot for Compton background measurement

fig, ax = plt.subplots(1, 1, figsize=set_size())

ax.scatter(thickness_com, rates_com, marker="x", label="Compton background")
ax.errorbar(thickness_com, rates_com, xerr=thickness_com_err,␣
↪yerr=rates_com_err, ecolor="black", ls="", capsize=3)

p_com, Vp_com = curve_fit(double_exp, thickness_com, rates_com, p0=[2, -2,␣
↪1, -0.1])
ax.plot(np.linspace(-0.5, 11, 100), double_exp(np.linspace(-0.5, 11, 100),␣
↪p_com[0], p_com[1], p_com[2], p_com[3]), label="double exp", color="green")
ax.plot(np.linspace(-0.5, 11, 100), double_exp(np.linspace(-0.5, 11, 100),␣
↪0, p_com[1], p_com[2], p_com[3]), label="background", color="red")

ax.legend()
ax.set_xlim(-0.5, 11)
ax.set_ylim(0, 4)
ax.set(ylabel="Rate $\dot{N}$ [Bq]", xlabel="thickness $d$ [mm]")

plt.tight_layout()
plt.savefig("4_4_compton.pdf", format="pdf", bbox_inches='tight')
```

```
plt.show()

R_com = p_com[2]
R_com_err = np.sqrt(Vp_com[2][2])
```

Acrylic glass

[ ]:
```
# Calculation of transmission in acrylic glass from experiment

R_a = 1520/600.110
R_a_err = np.sqrt(1520)/600.110
R_0 = 1901/600.131
R_0_err = np.sqrt(1901)/600.131


T = (R_a-R_com)/(R_0-R_com) #R_a/R_0
T_err = np.sqrt(R_a_err**2+T**2*R_0_err**2+(R_a+R_0-2*R_com)**2/
 ↪(R_0-R_com)**2*R_com_err**2)/(R_0-R_com) #np.
 ↪sqrt(R_a_err**2+T**2*R_0_err**2)/R_0
print(R_a, R_a_err, R_0, R_0_err, T, T_err)
```

[ ]:
```
# Calculation of transmission in acrylic glass from theory

murho = 1.1
murho_err = 0.3
rho = 1.19
d = 0.196
d_err = 0.002

T_theory = np.exp(-murho*rho*d)
T_theory_err = T_theory*np.
 ↪sqrt(rho**2*d**2*murho_err**2+rho**2*d_err**2*murho**2)
print(T_theory, T_theory_err)
```

[ ]:
```
# Define correction function on data using Compton background and acrylic␣
 ↪glass conciderations

def corrections(counts, time):
    R_0 = counts/time
    R_0_err = np.sqrt(counts)/time
    R = R_0/T-R_com #(R_0-R_com)/T
    R_err = np.sqrt(R_0_err**2/T**2+R_com_err**2+R**2*T_err**2)
    R_err_stat = R_0_err/T
    return R, R_err, R_err_stat
```

7.2.4 Velocity calibration

[ ]:
```
# Data for the velocity conciderations

v_prog = np.arange(1, 11)
time = np.array([79.9, 40.0, 26.8, 20.1, 15.8, 13.2, 11.4, 10.0, 8.8, 8.0])
```

```
v_meas = 80/time
v_meas_err = np.sqrt((1/np.sqrt(6))**2+(80*0.3/time)**2)/time
```

[ ]:
```
# Linear plot of the velocities

fig, ax = plt.subplots(1, 1, figsize=set_size())

ax.scatter(v_prog, v_meas, marker="x", label="calibration")
ax.errorbar(v_prog, v_meas, yerr=v_meas_err, ecolor="black", ls="",␣
↪capsize=3)

p_cal_v, Vp_cal_v = curve_fit(f, v_prog, v_meas)
x = np.linspace(0, 11, 1000)
mod = Modell(x,p_cal_v)
konf = Konfidenz(x,p_cal_v,Vp_cal_v)
ax.plot(x, mod, label="linear regression", color="green")
ax.plot(x, konf[0], linestyle="dashed", linewidth=1, color="grey",␣
↪label="confidence band")
ax.plot(x, konf[1], linestyle="dashed", linewidth=1, color="grey")
ax.fill_between(x, konf[0], konf[1], color="whitesmoke", alpha=0.5)

ax.legend()
ax.set_xlim(0, 11)
ax.set(ylabel = "Measured velocity [mm/s]", xlabel = "Setup velocity [mm/s]")

plt.tight_layout()
plt.savefig("4_3_velocity.pdf", format="pdf", bbox_inches='tight')
plt.show()

def calibration_v(velocity):
    v = velocity*p_cal[0]+p_cal[1]
    v_err = np.sqrt(velocity**2*Vp_cal[0, 0]+Vp_cal[1,␣
↪1]+2*velocity*Vp_cal[0][1])
    return v, v_err
```

[ ]:
```
# Measurement of the same velocity 10 times

ts = [16.07, 15.90, 15.84, 15.90, 15.93, 16.15, 16.17, 16.07, 15.88, 15.92]
t = np.mean(ts)
t_err = np.std(ts)/np.sqrt(10)
v = 80/t
v_err = np.sqrt(1/6+(80/t*t_err)**2)/t

print(v, v_err)
```

7.2.5 Stainless steel analysis

Fit to the data and Isomeric shift

[ ]:
```
# New fit functions using Gauss, Lorentz and Voigt
```

```
def gauss_fit(x, A, mu, sigma, B):
    return -A/(np.sqrt(2*np.pi)*sigma)*np.exp(-(x-mu)**2/(2*sigma**2))+B

def lorentz_fit(x, A, mu, gamma, B):
    return -A/np.pi*gamma/((x-mu)**2+gamma**2)+B

def voigt_fit(x, A, mu, sigma, gamma, B):
    return -A*voigt_profile((x-mu), sigma, gamma)+B
```

[ ]:
```
# New read in function directly combining all measurement points from␣
↪several measurements

import pandas as pd

def combine(array):
    array = array[array[:, 0].argsort()]
    i = 1
    while (i<len(array)):
        if array[i][0] == array[i-1][0]:
            array[i]+=array[i-1]
            array[i][0]*=0.5
            array = np.delete(array, i-1, 0)
        else:
            i += 1
    return array

def read_moess(file):
    data = pd.read_table(file, header=0, decimal=',', names=['velocity',␣
↪'time', 'counts'], engine='python')
    all_data = np.array(data)
    all_data = combine(all_data)
    return all_data
```

[ ]:
```
# Data read in for stainless steel

data_stainless_steel = read_moess("Moessbauer_Data.txt")

v_stst = data_stainless_steel[:, 0]
R_stst, R_stst_err, R_stst_stat = corrections(data_stainless_steel[:, 2],␣
↪data_stainless_steel[:, 1]/1000)

print("Total time:")
print(sum(data_stainless_steel[:, 1])/1000/3600)
```

[ ]:
```
# Plot for stainless steel

fig, ax = plt.subplots(1, 1, figsize=set_size())

ax.scatter(v_stst, R_stst, marker="x", label="Absorption in stainless steel")
ax.errorbar(v_stst, R_stst, yerr=R_stst_err, ecolor="black", ls="",␣
↪capsize=3, linewidth=1, label="Background uncertainty")
```

```
ax.errorbar(v_stst, R_stst, yerr=R_stst_stat, ecolor="slategrey", ls="",␣
 ↪capsize=3, linewidth=1, label="Statistical uncertainty")

p_stst_g, Vp_stst_g = curve_fit(gauss_fit, v_stst, R_stst, sigma=R_stst_err,␣
 ↪p0=[0.5, 0, 0.5, 1.0], absolute_sigma=True)
ax.plot(np.linspace(-2.6, 2.6, 1000), gauss_fit(np.linspace(-2.6, 2.6,␣
 ↪1000), *p_stst_g), label="Gauss", color="green")

p_stst_l, Vp_stst_l = curve_fit(lorentz_fit, v_stst, R_stst,␣
 ↪sigma=R_stst_err, p0=[0.5, 0, 0.5, 1.0], absolute_sigma=True)
ax.plot(np.linspace(-2.6, 2.6, 1000), lorentz_fit(np.linspace(-2.6, 2.6,␣
 ↪1000), *p_stst_l), label="Lorentz", color="blue")

p_stst_v, Vp_stst_v = curve_fit(voigt_fit, v_stst, R_stst, sigma=R_stst_err,␣
 ↪p0=[0.5, 0, 0.5, 0.5, 0.9], absolute_sigma=True, bounds=(0, np.inf))
ax.plot(np.linspace(-2.6, 2.6, 1000), voigt_fit(np.linspace(-2.6, 2.6,␣
 ↪1000), *p_stst_v), label="Voigt", color="red")


ax.legend()
ax.set(ylabel = "Rate $\dot{N}$ [Bq]", xlabel = "velocity $v$ [mm/s]")

plt.tight_layout()
plt.savefig("4_4_stainless_steel.pdf", format="pdf", bbox_inches='tight')
plt.show()
```

[ ]:
```
# Residual plot

fig, axs = plt.subplots(3, 1, figsize=set_size("page", subplots=(1, 2),␣
 ↪ratio=2.5))

axs[0].scatter(v_stst, R_stst-gauss_fit(v_stst, *p_stst_g), marker="x",␣
 ↪label="Data")
axs[0].errorbar(v_stst, R_stst-gauss_fit(v_stst, *p_stst_g),␣
 ↪yerr=R_stst_err, ecolor="black", ls="", capsize=3, linewidth=1,␣
 ↪label="Background uncertainty")
axs[0].errorbar(v_stst, R_stst-gauss_fit(v_stst, *p_stst_g),␣
 ↪yerr=R_stst_stat, ecolor="slategrey", ls="", capsize=3, linewidth=1,␣
 ↪label="Statistical uncertainty")
axs[0].set_title("Gauss")

axs[1].scatter(v_stst, R_stst-lorentz_fit(v_stst, *p_stst_l), marker="x",␣
 ↪label="Data")
axs[1].errorbar(v_stst, R_stst-lorentz_fit(v_stst, *p_stst_l),␣
 ↪yerr=R_stst_err, ecolor="black", ls="", capsize=3, linewidth=1,␣
 ↪label="Background uncertainty")
axs[1].errorbar(v_stst, R_stst-lorentz_fit(v_stst, *p_stst_l),␣
 ↪yerr=R_stst_stat, ecolor="slategrey", ls="", capsize=3, linewidth=1,␣
 ↪label="Statistical uncertainty")
axs[1].set_title("Lorentz")
```

```
axs[2].scatter(v_stst, R_stst-voigt_fit(v_stst, *p_stst_v), marker="x",␣
 ↪label="Data")
axs[2].errorbar(v_stst, R_stst-voigt_fit(v_stst, *p_stst_v),␣
 ↪yerr=R_stst_err, ecolor="black", ls="", capsize=3, linewidth=1,␣
 ↪label="Background uncertainty")
axs[2].errorbar(v_stst, R_stst-voigt_fit(v_stst, *p_stst_v),␣
 ↪yerr=R_stst_stat, ecolor="slategrey", ls="", capsize=3, linewidth=1,␣
 ↪label="Statistical uncertainty")
axs[2].set_title("Voigt")
ax.set(ylabel="Residuals [Bq]")

for ax in fig.get_axes():
        ax.legend()
        ax.set(ylabel="Residuals [Bq]")
        ax.set_xlim(-3,3)
        ax.axhline(0, color="black")

plt.tight_layout()
plt.savefig("4_4_stainless_steal_res.pdf", format="pdf", bbox_inches='tight')
plt.show()
```

[ ]:
```
# Calculation of isomeric shift

E_gam = 14.41295e3
E_gam_err = 0.31
h = 6.6260802e-34
c = 299792e6
e = 1.602177e-19

E_iso_stst_g = E_gam*p_stst_g[1]/c
E_iso_stst_g_err = np.
 ↪sqrt(E_gam**2*Vp_stst_g[1][1]+E_gam_err**2*p_stst_g[1]**2)/c
E_iso_stst_l = E_gam*p_stst_l[1]/c
E_iso_stst_l_err = np.
 ↪sqrt(E_gam**2*Vp_stst_l[1][1]+E_gam_err**2*p_stst_l[1]**2)/c
E_iso_stst_v = E_gam*p_stst_v[1]/c
E_iso_stst_v_err = np.
 ↪sqrt(E_gam**2*Vp_stst_v[1][1]+E_gam_err**2*p_stst_v[1]**2)/c
```

Effective absorber thickness

[ ]:
```
# Definition of constants and calculation of effective absorber thickness

f_A = 0.8 # 1
d_A = 25e-6 # m
beta = 0.022 # 1

frac = 0.7 # 1
frac_err = 0.05
N_A = 6.02214e23 # 1/mol
```

```
M = 55.845 # g/mol
M_err = 0.002
rho_steel = 7.874 # g/cm^3
n_A = rho_steel*N_A/M*frac*1e6 # 1/m^3
n_A_err = rho_steel*N_A/M*np.sqrt(frac_err**2+(1/M*frac*M_err)**2)*1e6

lam = h*c/E_gam/e/1000 # m
alpha = 8.58 # 1
alpha_err = 0.18
sigma_0 = lam**2/(2*np.pi)*2/(1+alpha)
sigma_0_err = lam**2/(2*np.pi)*2/(1+alpha)**2*alpha_err

T_A = f_A*n_A*beta*sigma_0*d_A
T_A_err = f_A*beta*d_A*np.sqrt((n_A_err*sigma_0)**2+(n_A*sigma_0_err)**2)
```

Debye-Waller-Factor

[ ]:
```
# Function calculating the DW factor for given parameters, uncertainties and␣
 ↪absorber thicknesses

from scipy.special import jv

def DW(p, Vp, pos_mu, func, T=T_A, T_err=T_A_err):
    B = p[-1]
    B_err_sq = Vp[-1][-1]
    A = B - func(p[pos_mu], *p)
    Amp_err = abs(func(p[pos_mu]+np.sqrt(Vp[pos_mu][pos_mu]),␣
 ↪*p)-func(p[pos_mu], *p))
    A_err_sq = B_err_sq+Amp_err**2
    DW = np.abs(A/B/(1-np.exp(-T_A/2)*jv(0, 1j*T_A/2)))
    DW_err = np.abs(np.sqrt((DW/A)**2*A_err_sq+(DW/B)**2*B_err_sq+
                            (A/B*np.exp(T/2)*(jv(0, 1j*T/2)+1j*jv(1, 1j*T/
 ↪2))/
                             (2*(np.exp(T/2)-jv(0, 1j*T/2))**2)*T_err)**2))
    return DW, DW_err

DW_g = DW(p_stst_g, Vp_stst_g, 1, gauss_fit)
DW_l = DW(p_stst_l, Vp_stst_l, 1, lorentz_fit)
DW_v = DW(p_stst_v, Vp_stst_v, 1, voigt_fit)
```

Lifetime

[ ]:
```
# Definition of constants and approximation of effective source thickness

d_Q = 100e-10 # m
beta_Q = 1 # 1
n_Q = n_A

T_Q = DW_v[0]*n_Q*beta_Q*sigma_0*d_Q
T_Q_err = DW_v[1]*n_Q*beta_Q*sigma_0*d_Q
```

[ ]:
```
# Function returning the correction factor on the width for a given absorber thickness

def width_correction(fwhm, fwhm_err, T=T_A, T_err=T_A_err):
    W = 2*(1+0.1288*T+4.733e-3*T**2-9.21e-4*T**3+3.63e-5*T**4)
    W_err = 2*(0.1288+2*4.733e-3*T-3*9.21e-4*T**2+4*3.63e-5*T**3)*T_err
    print("relative broadening:")
    print(W, W_err)
    return fwhm/W, np.sqrt((fwhm_err/W)**2+(fwhm/W**2*W_err)**2)
```

[ ]:
```
# Function doing the analysis for the lifetime: calculating FWHM and tau with and without the correction and calculating a t-value

def lifetime(gamma, gamma_err_sq, lorentz=True, voigt_sig=0, voigt_sig_err_sq=0, T=T_A, T_err=T_A_err):
    if lorentz:
        fwhm = 2*gamma
        fwhm_err = 2*np.sqrt(gamma_err_sq)
    elif voigt_sig != 0:
        fwhm_1 = 2*gamma
        fwhm_1_err = 2*np.sqrt(gamma_err_sq)
        fwhm_2 = 2*np.sqrt(2*np.log(2))*voigt_sig
        fwhm_2_err = 2*np.sqrt(2*np.log(2))*np.sqrt(voigt_sig_err_sq)
        fwhm = 0.5346*fwhm_1+np.sqrt(0.2166*fwhm_1**2+fwhm_2**2)
        fwhm_err = np.sqrt((0.5346+0.2166*fwhm_1/np.sqrt(0.2166*fwhm_1**2+fwhm_2**2))*fwhm_1_err)**2
                           +(fwhm_2/np.sqrt(0.2166*fwhm_1**2+fwhm_2**2))**2*fwhm_2_err)
    else:
        fwhm = 2*np.sqrt(2*np.log(2))*gamma
        fwhm_err = 2*np.sqrt(2*np.log(2))*np.sqrt(gamma_err_sq)
    print("FWHM in v")
    print(fwhm, fwhm_err)
    fwhm = E_gam*fwhm/c
    fwhm_err = E_gam*fwhm_err/c
    print("FWHM in energies")
    print(fwhm, fwhm_err)
    tau_0 = h/(2*np.pi)/fwhm/e
    tau_0_err = h/(2*np.pi)/fwhm**2*fwhm_err/e
    print("Lifetime")
    print(tau_0, tau_0_err)
    fwhm, fwhm_err = width_correction(fwhm, fwhm_err, T, T_err)
    print("Corrected FWHM")
    print(fwhm, fwhm_err)
    tau_0 = h/(2*np.pi)/fwhm/e
    tau_0_err = h/(2*np.pi)/fwhm**2*fwhm_err/e
    print("Corrected lifetime")
    print(tau_0, tau_0_err)
    t = abs(tau_0-141e-9)/tau_0_err
    print("t value")
```

```
    print(t)
    return tau_0, tau_0_err

tau_stst_l = lifetime(p_stst_l[2], Vp_stst_l[2][2])
```

[ ]:
```
# Plot with corrected FWHM

fig, ax = plt.subplots(1, 1, figsize=set_size())

ax.scatter(v_stst, R_stst, marker="x", label="Absorption in stainless steel")
ax.errorbar(v_stst, R_stst, yerr=R_stst_err, ecolor="black", ls="",␣
↪capsize=3, linewidth=1, label="Background uncertainty")
ax.errorbar(v_stst, R_stst, yerr=R_stst_stat, ecolor="slategrey", ls="",␣
↪capsize=3, linewidth=1, label="Statistical uncertainty")

ax.plot(np.linspace(-2.6, 2.6, 1000), lorentz_fit(np.linspace(-2.6, 2.6,␣
↪1000), *p_stst_l), label="Lorentz fit", color="black")

par_1 = h/(2*np.pi*tau_stst_l[0])/2/(E_gam*e)*c
ax.plot(np.linspace(-2.6, 2.6, 1000), lorentz_fit(np.linspace(-2.6, 2.6,␣
↪1000), p_stst_l[0]/p_stst_l[2]*par_1, p_stst_l[1], par_1, p_stst_l[3]),␣
↪label="corrected Lorentz", color="red")

par_2 = h/(2*np.pi*141e-9)/2/E_gam/e*c
ax.plot(np.linspace(-2.6, 2.6, 1000), lorentz_fit(np.linspace(-2.6, 2.6,␣
↪1000), p_stst_l[0]/p_stst_l[2]*par_2, p_stst_l[1], par_2, p_stst_l[3]),␣
↪label="theoretical Lorentz", color="green")

ax.legend()
ax.set(ylabel = "Rate $\dot{N}$ [Bq]", xlabel = "velocity $v$ [mm/s]")

plt.tight_layout()
plt.savefig("4_4_expectation.pdf", format="pdf", bbox_inches='tight')
plt.show()
```

7.2.6 Natural Iron analysis

Fit to the data

[ ]:
```
# Fit functions for sixfold models

def six_gauss_fit(x, A1, mu1, sigma1, A2, mu2, sigma2, A3, mu3, sigma3, A4,␣
↪mu4, sigma4, A5, mu5, sigma5, A6, mu6, sigma6, B):
    func = 0
    func -= A1/(np.sqrt(2*np.pi)*sigma1)*np.exp(-(x-mu1)**2/(2*sigma1**2))
    func -= A2/(np.sqrt(2*np.pi)*sigma2)*np.exp(-(x+mu2)**2/(2*sigma2**2))
    func -= A3/(np.sqrt(2*np.pi)*sigma3)*np.exp(-(x-mu3)**2/(2*sigma3**2))
    func -= A4/(np.sqrt(2*np.pi)*sigma4)*np.exp(-(x+mu4)**2/(2*sigma4**2))
    func -= A5/(np.sqrt(2*np.pi)*sigma5)*np.exp(-(x-mu5)**2/(2*sigma5**2))
    func -= A6/(np.sqrt(2*np.pi)*sigma6)*np.exp(-(x+mu6)**2/(2*sigma6**2))
    func += B
```

```
    return func

def six_lorentz_fit(x, A1, mu1, gamma1, A2, mu2, gamma2, A3, mu3, gamma3,␣
↪A4, mu4, gamma4, A5, mu5, gamma5, A6, mu6, gamma6, B):
    func = 0
    func -= A1/np.pi*gamma1/((x-mu1)**2+gamma1**2)
    func -= A2/np.pi*gamma2/((x+mu2)**2+gamma2**2)
    func -= A3/np.pi*gamma3/((x-mu3)**2+gamma3**2)
    func -= A4/np.pi*gamma4/((x+mu4)**2+gamma4**2)
    func -= A5/np.pi*gamma5/((x-mu5)**2+gamma5**2)
    func -= A6/np.pi*gamma6/((x+mu6)**2+gamma6**2)
    func += B
    return func

def six_voigt_fit(x, A1, mu1, sigma1, gamma1, A2, mu2, sigma2, gamma2, A3,␣
↪mu3, sigma3, gamma3, A4, mu4, sigma4, gamma4, A5, mu5, sigma5, gamma5, A6,␣
↪mu6, sigma6, gamma6, B):
    func = 0
    func -= A1*voigt_profile((x-mu1), sigma1, gamma1)
    func -= A2*voigt_profile((x+mu2), sigma2, gamma2)
    func -= A3*voigt_profile((x-mu3), sigma3, gamma3)
    func -= A4*voigt_profile((x+mu4), sigma4, gamma4)
    func -= A5*voigt_profile((x-mu5), sigma5, gamma5)
    func -= A6*voigt_profile((x+mu6), sigma6, gamma6)
    func += B
    return func
```

[ ]:
```
# Data import for natural iron

data_natural_iron = read_moess("Moessbauer_Iron.txt")

v_nair = data_natural_iron[:, 0]
R_nair, R_nair_err, R_nair_stat = corrections(data_natural_iron[:, 2],␣
↪data_natural_iron[:, 1]/1000)

print("Total time:")
print(sum(data_natural_iron[:, 1])/1000/3600)
```

[ ]:
```
# Plot for natural iron

init_guess_gl = [0.2, 0.8, 0.5, 0.2, 0.8, 0.5, 0.4, 3.1, 0.5, 0.4, 3.1, 0.5,␣
↪0.4, 5.2, 0.5, 0.4, 5.2, 0.5, 1.0]
init_guess_v = [0.2, 0.8, 0.5, 0.5, 0.2, 0.8, 0.5, 0.5, 0.4, 3.1, 0.5, 0.5,␣
↪0.4, 3.1, 0.5, 0.5, 0.4, 5.2, 0.5, 0.5, 0.4, 5.2, 0.5, 0.5, 1.0]

fig, ax = plt.subplots(1, 1, figsize=set_size())

ax.scatter(v_nair, R_nair, marker="x", label="Absorption in natural iron")
ax.errorbar(v_nair, R_nair, yerr=R_nair_err, ecolor="black", ls="",␣
↪capsize=3, linewidth=1, label="Background uncertainty")
```

```
ax.errorbar(v_nair, R_nair, yerr=R_nair_stat, ecolor="slategrey", ls="",␣
 ↪capsize=3, linewidth=1, label="Statistical uncertainty")

p_nair_g_1, Vp_nair_g_1 = curve_fit(six_gauss_fit, v_nair, R_nair,␣
 ↪sigma=R_nair_err, p0=init_guess_gl, absolute_sigma=True, bounds=(0, np.
 ↪inf))
ax.plot(np.linspace(-8, 8, 10000), six_gauss_fit(np.linspace(-8, 8, 10000),␣
 ↪*p_nair_g_1), label="Gauss", color="green")

p_nair_l_1, Vp_nair_l_1 = curve_fit(six_lorentz_fit, v_nair, R_nair,␣
 ↪sigma=R_nair_err, p0=init_guess_gl, absolute_sigma=True, bounds=(0, np.
 ↪inf))
ax.plot(np.linspace(-8, 8, 10000), six_lorentz_fit(np.linspace(-8, 8,␣
 ↪10000), *p_nair_l_1), label="Lorentz", color="blue")

p_nair_v_1, Vp_nair_v_1 = curve_fit(six_voigt_fit, v_nair, R_nair,␣
 ↪sigma=R_nair_err, p0=init_guess_v, absolute_sigma=True, bounds=(0, np.inf))
ax.plot(np.linspace(-8, 8, 10000), six_voigt_fit(np.linspace(-8, 8, 10000),␣
 ↪*p_nair_v_1), label="Voigt", color="red")


ax.legend()
ax.set(ylim = (0.6,1.25), xlim = (-8,8), ylabel = "Rate $\dot{N}$ [Bq]",␣
 ↪xlabel = "velocity $v$ [mm/s]")

plt.tight_layout()
plt.savefig("4_5_natural_iron.pdf", format="pdf", bbox_inches='tight')
plt.show()
```

[ ]:
```
# Residual plot

fig, axs = plt.subplots(3, 1, figsize=set_size("page", subplots=(1, 2),␣
 ↪ratio=2.5))

axs[0].scatter(v_nair, R_nair-six_gauss_fit(v_nair, *p_nair_g_1),␣
 ↪marker="x", label="Data")
axs[0].errorbar(v_nair, R_nair-six_gauss_fit(v_nair, *p_nair_g_1),␣
 ↪yerr=R_nair_err, ecolor="black", ls="", capsize=3, linewidth=1,␣
 ↪label="Background uncertainty")
axs[0].errorbar(v_nair, R_nair-six_gauss_fit(v_nair, *p_nair_g_1),␣
 ↪yerr=R_nair_stat, ecolor="slategrey", ls="", capsize=3, linewidth=1,␣
 ↪label="Statistical uncertainty")
axs[0].set_title("Gauss")

axs[1].scatter(v_nair, R_nair-six_lorentz_fit(v_nair, *p_nair_l_1),␣
 ↪marker="x", label="Data")
axs[1].errorbar(v_nair, R_nair-six_lorentz_fit(v_nair, *p_nair_l_1),␣
 ↪yerr=R_nair_err, ecolor="black", ls="", capsize=3, linewidth=1,␣
 ↪label="Background uncertainty")
```

```
axs[1].errorbar(v_nair, R_nair-six_lorentz_fit(v_nair, *p_nair_l_1),␣
 ↪yerr=R_nair_stat, ecolor="slategrey", ls="", capsize=3, linewidth=1,␣
 ↪label="Statistical uncertainty")
axs[1].set_title("Lorentz")

axs[2].scatter(v_nair, R_nair-six_voigt_fit(v_nair, *p_nair_v_1),␣
 ↪marker="x", label="Data")
axs[2].errorbar(v_nair, R_nair-six_voigt_fit(v_nair, *p_nair_v_1),␣
 ↪yerr=R_nair_err, ecolor="black", ls="", capsize=3, linewidth=1,␣
 ↪label="Background uncertainty")
axs[2].errorbar(v_nair, R_nair-six_voigt_fit(v_nair, *p_nair_v_1),␣
 ↪yerr=R_nair_stat, ecolor="slategrey", ls="", capsize=3, linewidth=1,␣
 ↪label="Statistical uncertainty")
axs[2].set_title("Voigt")
ax.set(ylabel="Residuals [Bq]")

for ax in fig.get_axes():
        ax.legend()
        ax.set(ylabel="Residuals [Bq]")
        ax.set_xlim(-8,8)
        ax.axhline(0, color="black")

plt.tight_layout()
plt.savefig("4_5_natural_iron_res.pdf", format="pdf", bbox_inches='tight')
plt.show()
```

Isomeric shift and Hyperfine structure and Magnetic field/moment

[ ]:
```
# Definiton of additional quantities

mu_n = 3.15245e-8
mu_g = 0.09044*mu_n
mu_g_err = 0.00007*mu_n
```

[ ]:
```
# Function doing analysis for Isomeric shift and Hyperfine structure:
# converting energies, finding isomeric shift and hyperfine states,␣
 ↪calculating magnetic field and moment

def IsoHyper(v, v_err_sq):
    print("energies:")
    E = E_gam*v/c
    E_err = E_gam*np.sqrt(v_err_sq)/c
    print(E, E_err)
    print("isomeric shift")
    E_isos = [(E[0]+E[1])/2, (E[2]+E[3])/2, (E[4]+E[5])/2]
    E_iso = np.mean(E_isos)
    E_iso_err = np.std(E_isos)/np.sqrt(3)
    print(E_iso, E_iso_err)
    E = E-E_iso
    E_err = np.sqrt(E_err**2+E_iso_err**2)
    E_34 = (E[0]-E[1])/2
```

```
    E_34_err = np.sqrt(E_err[0]**2+E_err[1]**2)/2
    E_25 = (E[2]-E[3])/2
    E_25_err = np.sqrt(E_err[2]**2+E_err[3]**2)/2
    E_16 = (E[4]-E[5])/2
    E_16_err = np.sqrt(E_err[4]**2+E_err[5]**2)/2
    print("E_34")
    print(E_34, E_34_err)
    print("E_25")
    print(E_25, E_25_err)
    print("E_16")
    print(E_16, E_16_err)
    print("magnetic field")
    B = (E_34+E_25)/(2*mu_g)
    B_err = np.sqrt(E_34_err**2+E_25_err**2+(2*B*mu_g_err)**2)/(2*mu_g)
    print(B, B_err)
    print("magnetic moment")
    mu_e = (mu_g-E_16/B)/mu_n
    mu_e_err = np.sqrt(mu_g_err**2+(E_16_err/B)**2+(E_16/B**2*B_err)**2)/mu_n
    print(mu_e, mu_e_err)
```

[ ]:
```
# Finding the mean peak veolcities that can be inserted in the IsoHyper␣
 ↪function

v_nair_g = np.array([p_nair_g_1[1], -p_nair_g_1[4], p_nair_g_1[7],␣
 ↪-p_nair_g_1[10], p_nair_g_1[13], -p_nair_g_1[16]])
v_nair_g_err = np.array(np.diag(Vp_nair_g_1)[1::3])
v_nair_l = np.array([p_nair_l_1[1], -p_nair_l_1[4], p_nair_l_1[7],␣
 ↪-p_nair_l_1[10], p_nair_l_1[13], -p_nair_l_1[16]])
v_nair_l_err = np.array(np.diag(Vp_nair_l_1)[1::3])
v_nair_v = np.array([p_nair_v_1[1], -p_nair_v_1[5], p_nair_v_1[9],␣
 ↪-p_nair_v_1[13], p_nair_v_1[17], -p_nair_v_1[21]])
v_nair_v_err = np.array(np.diag(Vp_nair_v_1)[1::4])#
```

Effective absorber thickness and Debye Waller factor

[ ]:
```
# Calculation of new effective absorber thickness

frac_nair = 0.98 # 1
frac_nair_err = 0.02
n_A_nair = rho_steel*N_A/M*frac_nair*1e6 # 1/m^3
n_A_nair_err = rho_steel*N_A/M*np.sqrt(frac_nair_err**2+(1/
 ↪M*frac_nair*M_err)**2)*1e6

T_A_nair = f_A*n_A_nair*beta*sigma_0*d_A
T_A_nair_err = f_A*beta*d_A*np.
 ↪sqrt((n_A_nair_err*sigma_0)**2+(n_A_nair*sigma_0_err)**2)
```

[ ]:
```
# Function doing analysis for Debye Waller factor:
# Calculate correction factor, effective absorber thickness and Debye Waller␣
 ↪for given parameters
```

```
def DW_nair(p, Vp, pos_mu, pos_A, func, N, N_err):
    print("correction factor:")
    W_j = p[pos_A]/N
    W_j_err = np.sqrt(Vp[pos_A][pos_A]+(p[pos_A]/N*N_err)**2)/N
    print(W_j, W_j_err)
    print("effective absorber thickness")
    T_A_j = W_j*T_A_nair
    T_A_j_err = np.sqrt(W_j_err**2+T_A_nair_err**2)
    print(T_A_j, T_A_j_err)
    print("Debye-Waller")
    DW_nair = DW(p, Vp, pos_mu, func, T=T_A_j, T_err=T_A_j_err)
    print(DW_nair)
    return T_A_j, T_A_j_err

N_g = sum(p_nair_g_1[:-1:3])
N_g_err = np.sqrt(sum(np.diag(Vp_nair_g_1)[:-1:3]))
N_l = sum(p_nair_l_1[:-1:3])
N_l_err = np.sqrt(sum(np.diag(Vp_nair_l_1)[:-1:3]))
N_v = sum(p_nair_v_1[:-1:4])
N_v_err = np.sqrt(sum(np.diag(Vp_nair_l_1)[:-1:4]))
```

Lifetimes

[ ]:
```
# Using previously defined functions, DW and lifetime can be found:
# Here example for first voigt peak is shown

i = 1

T_nair, T_nair_err = DW_nair(p_nair_v_1, Vp_nair_v_1, i*4-3, i*4-4,␣
↪six_voigt_fit, N_v, N_v_err)
tau = lifetime(p_nair_v_1[i*4-1], Vp_nair_v_1[i*4-1][i*4-1], lorentz=False,␣
↪T=T_A_nair, T_err=T_A_nair_err, voigt_sig=p_nair_v_1[i*4-2],␣
↪voigt_sig_err_sq=Vp_nair_v_1[i*4-2][i*4-2])
```

7.3 Lab notes

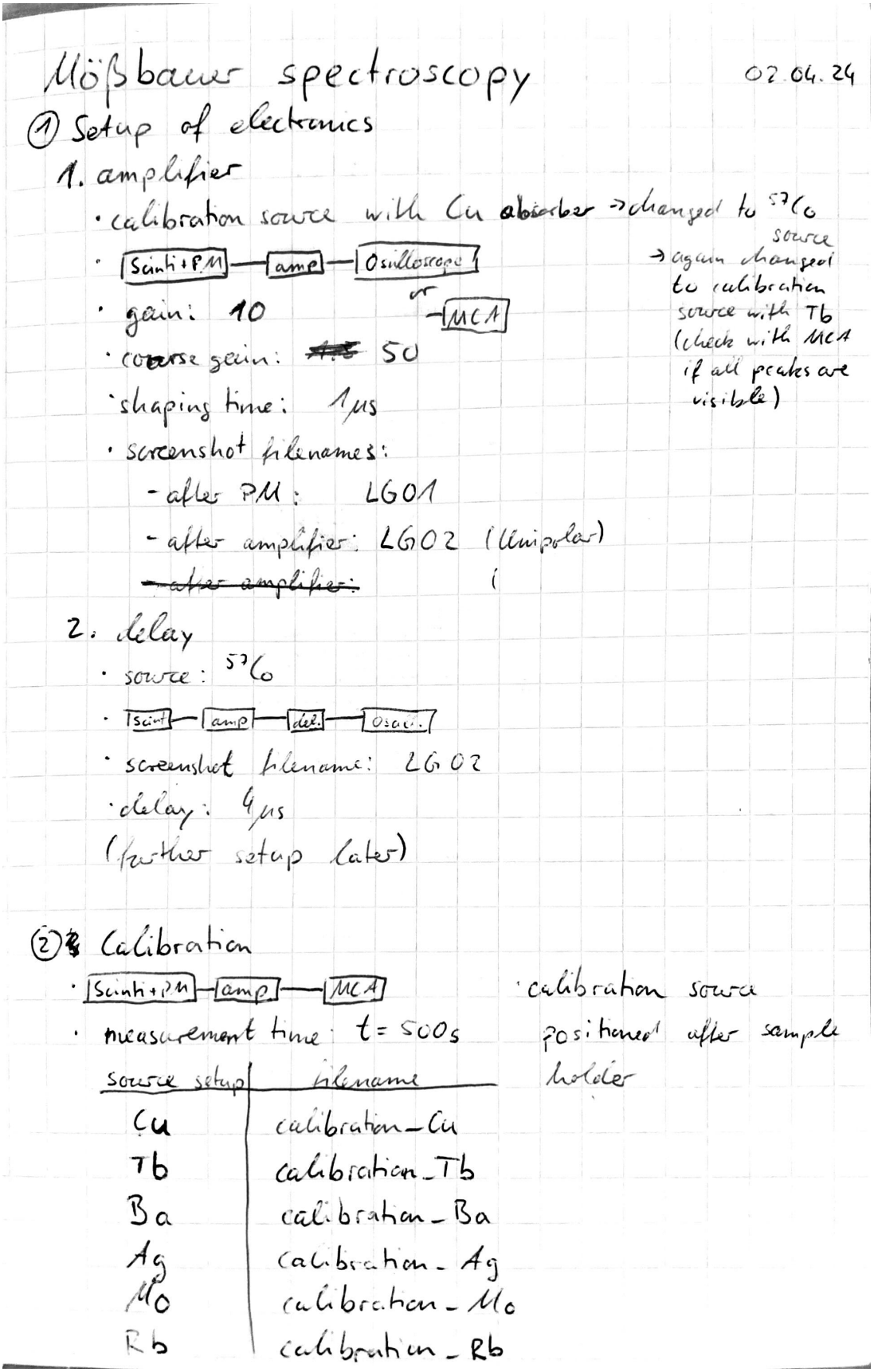

Mößbauer spectroscopy 02.04.24

① Setup of electronics

1. amplifier
   - calibration source with Cu absorber → changed to ^{57}Co source
   - Scinti+PM — amp — Oscilloscope / or — MCA
   - gain: 10
   - coarse gain: ~~1~~ 50
   - shaping time: 1 µs
   - screenshot filenames:
     - after PM: LG01
     - after amplifier: LG02 (unipolar)
     - ~~after amplifier:~~ (

→ again changed to calibration source with Tb (check with MCA if all peaks are visible)

2. delay
   - source: ^{57}Co
   - Scint — amp — del. — Osci.
   - screenshot filename: LG02
   - delay: 4 µs

(further setup later)

② Calibration
- Scinti+PM — amp — MCA
- measurement time: t = 500s
- calibration source positioned after sample holder

source setup	filename
Cu	calibration_Cu
Tb	calibration_Tb
Ba	calibration_Ba
Ag	calibration_Ag
Mo	calibration_Mo
Rb	calibration_Rb

③ ^{57}Co spectrum
- setup as in ② but with ^{57}Co source
- measurement time: $t = 3500.89\,s$
- file name: spectrum_Co

④ further setup of electronics
1. delay →
- ^{57}Co source

- filename: LG03 without delay
- filename: LG04 with ~~4~~ 2 µs delay

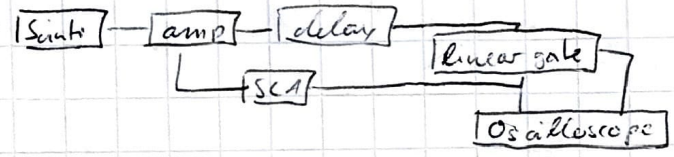

→ LG05 and LG06

2. SCA
- calibration source with Rb

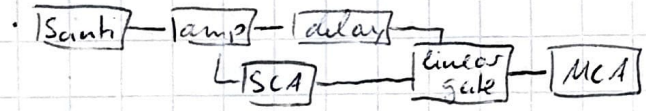

- delay of SCA: 1.28
- upper level: 1.00
- lower level: 0.72
- with ^{57}Co source: $t = 1960.86\,s$ filename: peak_Co

⑤ New amplification
- setup:

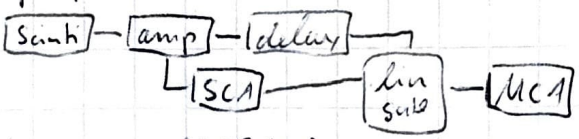

- SCA windows open (0.08 10.0) then lower energy window: 0.26
- amplification: coarse gain: 100 gain: 12.3

⑥ New Calibration
- setup as in ⑤
- measurement time: 750s

source setup	filename
Tb	calibration_Tb_2
Ba	calibration_Ba_2
Ag	calibration_Ag_2
Mo	calibration_Mo_2
Rb	calibration_Rb_2

⑦ New ^{57}Co Spectrum
- setup as in ⑤ but with ^{57}Co source
- t = 3292 s
- filename: spectrum_Co_2

⑧ SCA setup as in ⑥ ?.
- upper level: 2.42
- lower level: 1.54

⑨ Measurement without absorber
- setup as in ⑧ additional measurement
- t = 60515.95s t = 2235. 03.04.24
- filename peak_Co_error peak_Co_2
- additionally:

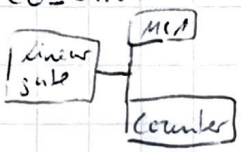

counts: ~~187253~~ 188048 (counts Left)
time: ~~57983~~ 57941s

(10) Background measurements

- Setup as in (8)
- with different shielding materials:
  - acrylic glass in sample holder
  - aluminium plates of ~~width~~ thickness d in front of Scintillator

~~Accounts~~ N	time t	shielding material	
1901	600.131s	no	
1520	600.110s	acrylic glass	d = 1.96mm ± 0.01mm (always error on d)
1436	604.373s	alu	d = 0.21mm
1095	600.346s	alu	d = 0.42mm (2 plates)
948	600.342s	alu	d = 0.63mm (3 plates)
792	600.266s	alu	d = 0.84mm (4 plates)
735	600.831s	alu	d = 1.01mm
681	600.122s	alu	d = 1.46mm
574	600.455s	alu	d = 1.96mm
641	602.663s	alu	d = 2.51mm
611	600.457s	alu	d = 3.01mm
580	600.146s	alu	d = 3.98mm
974	1045.33	alu	d = 4.99mm (2 plates)
541	599.559	alu	d = 5.94mm (2 plates)
538	601.123	alu	d = 6.99mm (2 plates)
525	605.357	alu	d = 7.91mm (2 plates)
499	600.432	alu	d = 8.99mm (3 plates)
517	600.154	alu	d = 9.94mm (3 plates)

(11) stainless steel

setup as in (8)

- with stainless steel in sample holder

1. start velocity $0.1 \frac{mm}{s}$
   step velocity $0.1 \frac{mm}{s}$
   end velocity $1.5 \frac{mm}{s}$
   measure time 150 s

various other measurements: 4.4.24

all parameters stored in file:
Moessbauer_data

(12) natural iron 5.4.24

- setup as in (8)
- with natural iron in sample holder
- measurements in file:
  Moessbauer_Iron

measurements of natural iron continued 8.4.24

measurement of natural iron continued 9.4.24

velocity calibration

distance: 8cm ± ~~1cm~~ 0.3cm

velocity	time	velocity	time
$1 \frac{mm}{s}$	79.9 s ± 0.3 s	$7 \frac{mm}{s}$	11.4 s ± 0.3 s
$2 \frac{mm}{s}$	40.0 s ± 0.3 s	$8 \frac{mm}{s}$	10.0 s ± 0.3 s
$3 \frac{mm}{s}$	26.8 s ± 0.3 s	$9 \frac{mm}{s}$	8.8 s ± 0.3 s
$4 \frac{mm}{s}$	20.1 s ± 0.3 s	$10 \frac{mm}{s}$	8.0 s ± 0.3 s
$5 \frac{mm}{s}$	15.8 s ± 0.3 s		
$6 \frac{mm}{s}$	13.2 s ± 0.3 s		

again measurement of stainless steal

velocity calibration, natural iron source 10.6.24

$d = 8\,cm \pm 0.1\,cm$

$v = 5\,\frac{mm}{s}$

$t_1 = 16.07\,s$
$t_2 = 15.90\,s$
$t_3 = 15.84\,s$
$t_4 = 15.90\,s$
$t_5 = 15.93\,s$
$t_6 = 16.15\,s$
$t_7 = 16.17\,s$
$t_8 = 16.07\,s$
$t_9 = 15.88\,s$
$t_{10} = 15.92$

measurement of stainless steal 11.6.24

measurement of natural iron

12.6.24

measurement of natural iron